



Published in final edited form as:

Mol Psychiatry. 2023 November ; 28(11): 4679–4692. doi:10.1038/s41380-023-02248-z.

Psychiatric risk gene Transcription Factor 4 (TCF4) regulates the density and connectivity of distinct inhibitory interneuron subtypes

Huei-Ying Chen¹, BaDoi N. Phan^{2,3,4}, Gina Shim¹, Gregory R. Hamersky¹, Norah Sadowski^{1,5}, Thomas S. O'Donnell¹, Srinidhi Rao Sripathy¹, Joseph F. Bohlen¹, Andreas R. Pfenning^{3,4}, Brady J. Maher^{1,5,6,✉}

¹Lieber Institute for Brain Development, Johns Hopkins Medical Campus, Baltimore, MD 21205, USA

²Computational Biology Department, School of Computer Science, Carnegie Mellon University, Pittsburgh, PA 15213, USA

³Neuroscience Institute, Carnegie Mellon University, Pittsburgh, PA 15213, USA

⁴Medical Scientist Training Program, University of Pittsburgh School of Medicine, Pittsburgh, PA 15261, USA

⁵Department of Psychiatry and Behavioral Sciences, Johns Hopkins University School of Medicine, Baltimore, MD 21287, USA

⁶The Solomon H. Snyder Department of Neuroscience, Johns Hopkins University School of Medicine, Baltimore, MD 21205, USA

Abstract

Transcription factor 4 (TCF4) is a basic helix-loop-helix transcription factor that is implicated in a variety of psychiatric disorders including autism spectrum disorder (ASD), major depression, and schizophrenia. Autosomal dominant mutations in TCF4 are causal for a specific ASD called Pitt-Hopkins Syndrome (PTHS). However, our understanding of etiological and pathophysiological mechanisms downstream of TCF4 mutations is incomplete. Single cell sequencing indicates TCF4 is highly expressed in GABAergic interneurons (INs). Here, we performed cell-type specific expression analysis (CSEA) and cellular deconvolution (CD) on bulk RNA sequencing data from 5 different PTHS mouse models. Using CSEA we observed differentially expressed genes (DEGs)

Reprints and permission information is available at <http://www.nature.com/reprints>

✉ **Correspondence** and requests for materials should be addressed to Brady J. Maher. brady.maher@libd.org.

AUTHOR CONTRIBUTIONS

H-YC and GS performed IHC and confocal imaging; H-YC, GS, TSO, SRS and JFB performed image analysis. H-YC and GRH performed electrophysiology experiments; H-YC and SRS performed qPCR and analysis. BNP performed RNA sequencing and ChIP-seq analysis under ARP supervision. NS performed RNA sequencing analysis on E13.5 samples. H-YC, GS and JFB performed mouse genotyping and colony maintenance. H-YC and BJM contributed to experimental design, data analyses and writing. All authors discussed the results and edited the manuscript.

COMPETING INTERESTS

The authors declare no competing interests.

Supplementary information The online version contains supplementary material available at <https://doi.org/10.1038/s41380-023-02248-z>.

were enriched in parvalbumin expressing (PV+) INs and CD predicted a reduction in the PV+ INs population. Therefore, we investigated the role of TCF4 in regulating the development and function of INs in the *Tcf4^{+/tr}* mouse model of PTHS. In *Tcf4^{+/tr}* mice, immunohistochemical (IHC) analysis of subtype-specific IN markers and reporter mice identified reductions in PV+, vasoactive intestinal peptide (VIP+), and cortistatin (CST+) expressing INs in the cortex and cholinergic (ChAT+) INs in the striatum, with the somatostatin (SST+) IN population being spared. The reduction of these specific IN populations led to cell-type specific alterations in the balance of excitatory and inhibitory inputs onto PV+ and VIP+ INs and excitatory pyramidal neurons within the cortex. These data indicate TCF4 is a critical regulator of the development of specific subsets of INs and highlight the inhibitory network as an important source of pathophysiology in PTHS.

INTRODUCTION

Transcription factor 4 (TCF4; not T-Cell Factor 4 which is encoded by *TCF7L2*) is a basic helix-loop-helix (bHLH) transcription factor (TF) implicated in a variety of psychiatric disorders including autism spectrum disorder (ASD), major depression, post-traumatic stress disorder, bipolar disorder, and schizophrenia [1]. Autosomal dominant mutations in TCF4 result in Pitt-Hopkins Syndrome (PTHS), a rare form of ASD characterized by developmental delay, intellectual disability, absent or limited speech, distinct facial features, motor delays, and gastrointestinal issues [2]. A subset of PTHS patients also experience breathing abnormalities and seizures [3, 4]. Beyond these clinical characteristics and their association to mutations in TCF4, our understanding of the pathophysiology and mechanisms downstream of mutations in TCF4 is not complete, and no specific therapeutics exist to treat PTHS.

TCF4 is a critical transcriptional regulator of many aspects of brain development and function [2]. In the mouse and human brain, bulk RNA sequencing analysis indicates that *TCF4* expression is developmentally regulated, peaking during the end of cortical neurogenesis then subsiding to a lower but stable level of expression throughout the lifespan [5, 6]. In the postnatal mouse brain, *Tcf4* expression is regional and cell-type specific, with expression observed in excitatory and inhibitory neurons, astrocytes, and throughout the oligodendrocyte lineage [7]. Across all cell types that express *Tcf4* in the adult mouse brain, *Tcf4* is most highly expressed in all major classes of GABAergic interneurons (INs) [8, 9]; however, our understanding of TCF4's role in IN development and function is lacking.

Coordination between INs and excitatory neurons is required to balance excitation and inhibition within brain circuits and for the generation of synchronous oscillations [10]. When dysregulated, these processes are associated with neuropsychiatric disorders including epilepsy, schizophrenia, and ASD [11–14]. INs are an exceedingly diverse population of neurons with individual subtypes showing distinct or partially overlapping morphological, electrophysiological, neurochemical, and transcriptomic profiles [15], and can be subdivided into three major categories based on expression of parvalbumin (PV), somatostatin (SST), or serotonin 3a receptor (5HT3aR) [16, 17]. Cortistatin (CST) expressing INs are an additional subtype of INs that partially overlap with PV+ and SST+ INs [18]. During mouse brain

development, INs are derived from ventral neuroprogenitor cells, with the vast majority of INs differentiating from medial and caudal ganglionic eminences (MGE, CGE) where they then tangentially migrate into the cortex [19].

Given the elevated expression of TCF4 across IN populations and the convergent role of INs and TCF4 in neuropsychiatric risk, we hypothesized that mutations in *Tcf4* could alter the development and/or function of INs in the mouse cortex. In this study, we surveyed IN development and function in a mouse model of PTHS which harbors a heterozygous truncating mutation in *Tcf4* [5]. Transcriptomic analysis and immunohistochemistry (IHC) demonstrated that TCF4 is an important regulator of distinct subsets of INs in cortical and subcortical regions in the mouse brain. In addition, electrophysiology showed that TCF4 mutation disrupted the excitatory-inhibitory balance by differentially affecting the frequency of inhibitory and/or excitatory synaptic inputs depending on the postsynaptic target. Together these results identify IN dysfunction as a potential pathophysiology underlying PTHS and other neuropsychiatric disorders associated with TCF4.

RESULTS

At the cellular level, *Tcf4* is broadly expressed in both neuronal and glial populations with the highest expression levels observed in GABAergic INs (Supplementary Fig. 1C) [7, 8]. Moreover, in situ hybridization against *Tcf4* in embryonic mouse brain sections demonstrated that *Tcf4* is highly expressed in the proliferative zones of the ventral pallidum which gives rise to cortical and subcortical INs (Supplementary Fig. 1A, B) [20]. To identify how mutations in TCF4 impact gene expression during embryonic development, we collected RNA from embryonic E13.5 *Tcf4*^{+/*tr*} and WT brains and performed RNA sequencing. Differential expression analysis identified 8 differentially expressed genes (DEG; padj<0.05), with *Tcf4* being the top DEG (Supplementary Table 1). Gene set enrichment analysis of downregulated DEGs ($p < 0.005$), identified enrichment for many general terms related to forebrain development such as regulation of neurogenesis, regulation of neuron differentiation, axonogenesis, and forebrain cell migration (Supplementary Fig. 2). In addition, we identified GO terms related to GABAergic neuron differentiation (Supplementary Fig. 2), cerebral cortex GABAergic IN, and IN migration (Supplementary Table 2). Given the expression of *Tcf4* within neuroprogenitor cells of the ganglionic eminences, the dysregulation of genes related to IN differentiation, and the elevated expression of *Tcf4* in the IN population, we next surveyed differential gene expression in the adult mouse brain in relation to INs.

We previously performed transcriptomic analysis on five different PTHS mouse models, collectively referred to as *Tcf4*^{+/*mut*}, and showed that cell-type specific expression analysis (CSEA) and cellular deconvolution (CD) was effective at identifying biological deficits in the oligodendrocyte population [6]. Therefore, using updated single cell sequencing datasets which contain greater cell-type specificity we re-analyzed our transcriptomic data [21]. Consistent with our prior report, oligodendrocytes showed the greatest enrichment of differentially expressed genes (DEGs), however this new analysis also revealed a specific enrichment of DEGs in PV+ INs (Fig. 1A). CD also predicted a marginally significant reduction in the proportion of PV+ INs across several PTHS mouse models (Fig. 1B, FDR

= 0.0645). This predicted reduction of PV+ INs was the second largest difference, with the largest effect size being attributed to a reduction in mature oligodendrocytes, a result that confirms our prior analysis [6]. The specificity for PV+ INs was notable because *Tcf4* expression is relatively consistent across all IN subtypes (Fig. 1C, Supplementary Fig. 1C). In addition, we updated our prior gene set enrichment analyses by testing for enrichment of synaptic genes with SynGO [22]. We found the PTHS mouse DEGs were significantly enriched for genes related to the synapse (FDR = 6.78×10^{-12}). These genes are further enriched in synaptic sub processes related to the postsynaptic density, synapse assembly, and regulation of neurotransmitter levels (Supplementary Fig. 3, Supplementary Table 3). Overall, these transcriptomic results, across development and within specific cellular populations, suggest that TCF4 is an important transcriptional regulator of IN development and synaptic function.

During brain development, bHLH TFs regulate cell proliferation, neuronal differentiation, and fate specification [23]. Canonically, TCF4 regulates transcription by forming homodimers or heterodimers with proneural class II bHLH TFs, however dimerization with non-bHLH TFs is reported [24–26]. In addition, co-occupancy of TFs on DNA is also known to regulate gene expression [27, 28], and enrichment of FOS/JUN DNA binding motifs were found to co-occur with TCF4 binding sites in human medial ganglionic eminence-like organoids [26]. We performed a similar analysis to infer which TFs may co-bind with TCF4 by re-analyzing three published TCF4 ChIP-seq datasets from SH-SY5S cell line [29–31]. We identified 13 candidate co-bound TFs that were consistently predicted across these datasets (maximum FDR = 0.004, Supplementary Table 4). Eight of these TFs were expressed in a single nucleus RNA-seq dataset of the human prefrontal cortex [32] and their expression was correlated with TCF4 expression in annotated INs, projection neurons, and glia (Supplementary Fig. 4). Of these top predicted co-bound TFs, we highlight ASCL1 (or MASH1), which is a class II bHLH TF that dimerizes with TCF4 [33–35] and is known to specify and promote differentiation of INs [36–38]. Together, these ChIP-seq analyses identify potential candidate TFs that may dimerize with TCF4 or co-bind DNA in close proximity to TCF4 and regulate gene expression in cortical INs.

To begin to understand the role of TCF4 in IN development and function we quantified IN populations in the *Tcf4^{+/-tr}* mouse model of PTHS [5]. We first compared the expression of IN markers by performing qPCR on whole brain lysates from *Tcf4^{+/-tr}* and WT littermates and observed a significant decrease in expression of the IN markers *Gad1*, *Gabra1*, *Pvalb*, and *Sst* (Fig. 2A). Next, we performed immunohistochemistry to quantify the density of specific IN populations in the cortex of WT and *Tcf4^{+/-tr}* littermates. We observed that cortical brain sections from *Tcf4^{+/-tr}* showed a significant reduction in GABA+ INs (Fig. 2B–D), and this appeared to be due to a specific reduction in the density of PV+ INs, as the density of SST+ INs was not altered (Fig. 2D).

To determine if these results are indicative of altered expression of IN-specific genes or reductions in specific IN populations, we next quantified IN density using subtype-specific reporter mice. IN subtypes can be broadly specified into three groups based on their expression of PV, SST, and 5HT3aR, with the 5HT3aR being further subdivided by expression of VIP [16]. The CST expressing INs is a unique population that overlaps with

PV+ and SST+ INs [18]. To examine these IN subtypes, we crossed promoter-specific cre lines (PV-cre, SST-cre, VIP-cre, and CST-cre) with a loxP-gated TdTomato reporter line (TdTom) and generated PV:TdTom, SST:TdTom, VIP:TdTom, and CST:TdTom reporter mice. These reporter mice were then crossed with *Tcf4*^{+/tr} mice to quantify subtype-specific IN densities in WT and *Tcf4*^{+/tr} mice. We observed a significant reduction in the density of PV+ and VIP+ populations in the M1 region of the motor cortex, but again the SST+ population was spared (Fig. 3B–D). We also observed a significant reduction in the density of CST+ INs (Fig. 3E). A similar reduction in the density of PV+ INs was also observed in the medial prefrontal cortex (mPFC); however, the VIP+ and SST+ INs populations remained unchanged (Fig. 3F–H).

The MGE and CGE also give rise to INs that populate subcortical brain regions [39–41]. Therefore, we also quantified the densities of INs populations in the striatum (Fig. 4A–C) and basal lateral amygdala (BLA; Fig. 4D–F). Again, we observed a significant reduction in the PV+ and VIP+ populations in both the striatum and BLA, with no effect of *Tcf4* mutations on the density of the SST population. Within the striatum, we also quantified the density of cholinergic INs, a striatal specific subpopulation of INs that express choline acetyltransferase (ChAT), using immunostaining for ChAT. The ChAT+ population was also significantly reduced in *Tcf4*^{+/tr} mice compared to WT littermates (Fig. 4G). Together, these results indicate that TCF4 is a critical regulator of differentiation and/or survival of specific subsets of INs in the mouse brain, having effects on the density of PV+, VIP+, CST+, and ChAT+ INs.

We next determined if TCF4 had any cell autonomous effects on the intrinsic excitability of INs and whether the observed reductions in IN density had any functional consequence on spontaneous network activity. We first recorded from layer 2/3 (L2/3) PV+ INs in acute brain slices of the mPFC and quantified intrinsic membrane properties and excitability. We observed no difference in the membrane capacitance, membrane resistance, or resting membrane potential between WT and *Tcf4*^{+/tr} PV+ INs (Fig. 5B–D). A consistent physiological property of PV+ INs is their ability to sustain high frequency firing with little or no adaptation and therefore are typically referred to as fast-spiking INs [42]. Using the current-clamp configuration, we elicited trains of action potentials (APs) in response to depolarizing current injection and observed that both WT and *Tcf4*^{+/tr} PV+ INs were capable of generating high frequency trains of APs (Fig. 5A). We observed no effect of *Tcf4* genotype on the frequency of AP output in response to increasing current steps (Fig. 5A), suggesting that although the density of PV+ INs is reduced, the intrinsic excitability of PV+ INs remains intact. Next, in the voltage-clamp configuration, we recorded spontaneous excitatory synaptic currents (sEPSCs) in PV+ INs by holding the neurons at –70 mV in the presence of gabazine, a GABA receptor antagonist, and observed no difference in the frequency or amplitude of sEPSCs between WT and *Tcf4*^{+/tr} PV+ INs (Fig. 5E), suggesting that excitatory inputs onto PV+ INs remain intact. To examine inhibitory connections onto PV+ INs, we recorded from PV+ INs using a potassium chloride (KCl)-based internal solution so that inward spontaneous inhibitory synaptic currents (sIPSCs) could be recorded at –70 mV. Consistent with the observed reduction in the density of INs, we observed a significant reduction in the frequency of sIPSCs in *Tcf4*^{+/tr} PV+ INs, but no difference in the sIPSC amplitude (Fig. 5F). These results suggest that inhibition onto PV+ INs appears to be

disrupted in the PTHS mouse model, likely due to the reduced densities of PV+ INs which are known to make recurrent synaptic connection onto nearby PV+ INs [43–47].

Following a similar paradigm, we recorded from VIP+ INs in L2/3 of the mPFC in acute brain slices. We observed no differences in the membrane capacitance or RMP, however we did observe that *Tcf4^{+/-tr}* VIP+ INs showed a significant increase in membrane resistance (Fig. 6B–D). The AP firing pattern of VIP+ INs is known to be heterogeneous [48], but we did not observe any gross differences in the AP firing patterns in the population of VIP+ INs we recorded and there was no difference in the frequency of AP output in response to increasing current steps (Fig. 6A). We next quantified sEPSCs recorded from VIP+ INs and observed a significant decrease in the sEPSC frequency with no differences in the sEPSC amplitude (Fig. 6E), indicating a reduction of excitatory input onto *Tcf4^{+/-tr}* VIP+ INs. Contrary to PV+ INs, VIP+ INs showed no difference in sIPSC frequency or amplitude (Fig. 6F), indicating that inhibitory inputs onto VIP+ INs remains intact in the mPFC of *Tcf4^{+/-tr}* mice. Together, these results indicate that VIP+ INs in the *Tcf4^{+/-tr}* mice show increased input resistance and reduced frequency of sEPSCs which indicates the excitatory drive onto VIP+ INs is reduced, and this may be slightly counterbalanced by an increase sensitivity/responsiveness to synaptic inputs due to the increased input resistance.

Lastly, we determined if the reduction in IN density was reflected in the balance of excitatory and inhibitory inputs onto pyramidal cells in the mPFC. Prior studies of both human and mouse models of PTHS have reported a reduction in spontaneous excitatory synaptic transmission and excitatory synapses [49–52]. Consistent with these prior results, we observed that pyramidal neurons in brain slices from *Tcf4^{+/-tr}* mice showed a significant reduction in the frequency and amplitude of sEPSCs compared to WT pyramidal cells (Fig. 7A). Next, we recorded sIPSCs from pyramidal cells at –70 mV with a KCl internal solution, and observed a reduction in the frequency and amplitude of sIPSC in *Tcf4^{+/-tr}* mice compared to WT neurons (Fig. 7B). The most parsimonious explanation for the reduction in sIPSC frequency is that it is related to the reduced density of INs in the mPFC. However, because the frequency of sEPSCs was also reduced, it suggests that the overall excitability of the mPFC and/or synaptic connectivity may be reduced, which could also contribute to the reduction in sIPSC frequencies. Therefore, to separate these potential mechanisms, we blocked spontaneous APs (i.e., excitability) with bath applied TTX and used a modified cesium methanesulfonate internal solution to record the frequency and amplitude of miniature EPSCs (mEPSCs) and mIPSCs in pyramidal neurons of the mPFC. Remarkably, in the presence of TTX, we observed no genotype differences in the frequency or amplitude of mEPSCs (Fig. 7C), which indicates excitatory synaptic connectivity is not altered in the mPFC of *Tcf4^{+/-tr}* mice. However, consistent with the reduced density of PV+ INs, the reduction in mIPSC frequency remained while mIPSC amplitude was no longer different by genotype (Fig. 7D). Together, these results suggest that deficits in the frequency and amplitude of sEPSCs in the mPFC of *Tcf4^{+/-tr}* mice appear to result from an overall reduction in spontaneous network excitability and not synaptic connectivity, whereas the main source of reduced sIPSC frequency onto pyramidal neurons is related to reduced IN densities. In summary, these results identify TCF4 as a critical regulator of IN density within the brain which leads to an overall reduction in network excitability in the cortex of the PTHS mouse model.

DISCUSSION

An imbalance between excitation and inhibition is a leading pathophysiological hypothesis for ASD [12, 53]. Here, we demonstrate in a mouse model of PTHS that mutations in *Tcf4* results in a significant reduction in the density of distinct IN subtypes in the cortex, BLA, and striatum resulting in abnormal spontaneous network activity. CSEA and CD of bulk RNA sequencing data highlighted transcriptomic alterations that were enriched in PV+ INs and qPCR of postnatal brain samples identified reductions in GABA-specific transcripts. IHC of GABA markers and GABA-specific reporter mice identified reductions in PV+, VIP+, CST+, and ChAT+ IN populations in *Tcf4^{+/-}* mice. Lastly, we demonstrated that the reduction of IN density was congruent with observed alterations in spontaneous synaptic activity and the known connectivity patterns of the postsynaptic cell-types we recorded. Altogether, we propose that the TCF4-dependent effects on IN density disrupts the balance of excitation and inhibition by decreasing the overall network excitability of the mPFC.

IN development and TCF4

During cortical development, INs are derived from three proliferative zones of the ventral pallidum, known as the lateral (LGE), medial (MGE), and caudal ganglionic eminence (CGE). The progenitor cells of the MGE and CGE are the primary source of INs, with the majority of PV+, SST+ and striatal INs originating from the MGE, while VIP+ INs primarily originate from the CGE [41, 54]. Cell-type specification of INs requires a complex interaction between intrinsic genetic programming and activity-dependent mechanisms, but whether specification is determined at the progenitor cell stage or after they migrate to their final position in the cortex is not fully understood [55]. Following IN migration, there is a period of developmental cell death that peaks around postnatal day 7 and eliminates approximately 40% of the developing cortical INs in a Bax-dependent manner [56]. *Tcf4* is expressed in the MGE, LGE and CGE during cortical development and maintains expression across all IN populations into adulthood (Supplementary Fig. 1), suggesting that mutations in *Tcf4* could disrupt any of these developmental stages. TCF4 was previously shown to be critical to many of these developmental stages for excitatory neurons, including dorsal progenitor proliferation, neurogenesis in the hippocampus, pyramidal cell fate specification, and pyramidal cell migration [50, 52, 57–62]. In addition, TCF4 is an activity-dependent TF which allows it to modify transcription in response to these developmentally instructive signals [34, 63–67]. Although this is the first direct evidence for TCF4 regulation of IN density in a mouse model of PTHS, it is consistent with a prior mouse study that showed TCF4 was highly specific to PV+IN epigenomes, as TCF4 binding motifs were enriched within ATAC-seq peaks of PV+ INs of the cortex, striatum, and the external globus pallidus [68]. Moreover, our results complement a human induced pluripotent stem cell (hiPSC) study that showed GABAergic organoid differentiation of a PTHS patient hiPSC line produced a lower percentage of GABAergic neurons compared to a parental control line [50]. TCF4 is also known to regulate the density of oligodendrocytes [6, 33, 69]. Which is an interesting point of convergence, considering that PV+ INs are heavily myelinated [70–72], and the first wave of MGE-derived oligodendrocyte precursor cells undergo developmental cell death at a similar developmental time point as INs [56, 73, 74].

The exact timing and mechanism(s) leading to these TCF4-dependent reductions in specific IN populations are not determined by our study and will require additional experimentation. However, based on the location and timing of *Tcf4* expression, its previously identified roles in excitatory neuronal development, and the stages of IN development, we predict this TCF4-dependent IN phenotype evolves between the start of IN-genesis and the second postnatal week, involving either ventral progenitor cells and/or immature INs. Interestingly, a prior publication showed embryonic reinstatement of *Tcf4* glutamatergic neurons (*Tcf4*^{STOP/+}::*Neurod6-Cre*) resulted in rescue of several behavior abnormalities (novel object location memory, anxiety, and nest building), however *Tcf4* reinstatement in GABAergic INs via *Gad2* promoter (*Tcf4*^{STOP/+}::*Gad2-Cre*) only showed a modest improvement in nest building [75]. The underlying mechanism(s) for these differential effects on behavioral normalization is complex, however it would be informative to quantify IN density in the *Tcf4*^{STOP/+}::*Gad2-Cre* mice. *Gad2* expression in the MGE appears to begin as neural progenitors transition to becoming INs [76], and therefore this *Tcf4* reinstatement could help determine if this IN density phenotypes occur in ventral progenitors or committed INs. Understanding at which stage(s) TCF4 mutations are producing this phenotype will not only inform us about disease mechanisms in PTHS, but will also provide important insights into molecular regulation of the development of specific subtypes of INs in the cortex.

PTHS and epilepsy

The prevalence of epilepsy in PTHS is estimated between 37–50% [3, 77], with a similar proportion of patients showing abnormal EEG with no distinctive characterization [78]. In PTHS mouse models, no evidence of seizure activity has been reported; however, local field potential (LFP) recordings and EEG have identified abnormalities in brain activity. For instance, LFP recordings in the hippocampus of awake behaving PTHS mice identified significant deficits in LFP power in the theta, beta, and gamma bands [75], and abnormalities in gamma frequency coherence and the latency of theta frequency coherence was observed in response to auditory evoked potentials [79]. These gamma band abnormalities are consistent with reduced density of PV+ INs, as gamma band oscillations are known to be associated with PV + IN function [80, 81].

Given the clinical presence of epilepsy in a subset of PTHS patients and the reduction of IN density reported here, it may seem surprising that seizure activity has not been reported in PTHS mouse models. However, the majority of mouse studies of PTHS have utilized the C57/BL6 mouse strain, which is known to be resistant to seizure activity [82]. Moreover, we observed an overall reduction in the frequency and amplitude of sEPSCs in pyramidal neurons of the mPFC, which is consistent with prior reports of deficits in synaptic and intrinsic excitability in both human and mouse models of PTHS [2, 49–52]. Therefore, we suggest the lack of seizure activity in the PTHS mouse model results from the reduced density of INs that leads to a reduction in network excitability, potentially through disinhibition of the IN network (see below).

Circuit abnormalities

The wiring diagrams of excitatory and inhibitory neurons in cortical microcircuits is highly complex with IN subtypes showing connectivity preferences for targeting specific

subcellular domains of specific postsynaptic target cell types, and is variable depending on the cortical layer and species [16, 43, 44, 46, 47, 83, 84]. Based on the data presented here and these prior neuronal connectivity studies, we suggest the reductions in spontaneous inhibitory and excitatory synaptic activity in the PTHS mouse model reflects the reduced density of the specific INs subtypes we identified and their well established ability to inhibit the inhibitory network (i.e., disinhibition). In PV + IN recordings we observed a reduction in the frequency of sIPSCs (Fig. 5F), which could result from the reduced densities of PV+ INs, as PV+ INs are known to have recurrent inhibitory connections [43, 47]. In recordings of VIP+ INs we showed no genotype effect on sIPSC frequencies and this appears to be related to the normal density of SST+ INs, as SST+ INs are the primary source of inhibition onto VIP+ INs [44, 47]. In pyramidal neuron recordings, we observed a reduction in the frequency of both sIPSC and mIPSCs, and this likely relates to the reduced density of PV+ INs, as this population of INs strongly regulate pyramidal cell excitation by preferentially synapsing onto the soma, perisomatic region, and action initial segments [44, 47]. In both pyramidal neurons and VIP+ INs, we observed a decrease in the frequency of sEPSCs, a result consistent with prior studies in human and mouse models of PTHS that show an overall reduction in excitatory network activity and intrinsic excitability [2, 49–51, 57]. However, our pyramidal cell recordings in the presence of TTX indicate that the reductions in spontaneous network activity (i.e., sEPSC frequency) are not due to deficits in excitatory synaptic connectivity or synaptic strength because we observed no genotype differences in mEPSC frequency or amplitude (Fig. 7). Rather, we posit that the overall reduction of spontaneous network excitability in the *Tcf4^{+tr}* mouse model in part reflects elevated inhibition of pyramidal cells due to the reduced densities of VIP+ and PV+ INs, which in turn leads to decreased disinhibition of INs and increased inhibition of pyramidal cells. Together, these results suggest that in addition to previously identified cell autonomous effects of TCF4 mutations on the excitability of cortical pyramidal cells, it also appears that reduced density of specific cortical IN populations leads to non-cell autonomous effects on pyramidal cell excitability.

In summary, we provide evidence that indicates TCF4 is an important regulator of differentiation and/or survival of specific subtypes of INs. Specifically, we show that TCF4 is highly expressed in ventral proliferative zones during development and across all IN populations into adulthood. Loss of TCF4 function resulted in reductions in PV+, VIP+, CST+, and ChAT+ INs in both cortical and subcortical regions. In the cortex, this resulted in altered spontaneous network activity that was specific to the neuronal subtype being recorded. Overall, these effects on the inhibitory network disturbs the balance of excitation and inhibition in the cortex of the *Tcf4^{+tr}* mouse model and may represent an important pathophysiological mechanism in PTHS patients.

MATERIALS AND METHODS

Animals and tissue collection

CST-cre (Cst-T2A-Cre) listed as Cort^{*tm1(cre)Zjh*}/J (Jackson Laboratory strain # 010910); PV-cre listed as B6.129P2-*Pvalb^{tm1(cre)Arbr}*/J (Jackson Laboratory strain #:017320); SST-cre listed as B6J.Cg-Sst^{*tm2.1(cre)Zjh*}/MwarJ (Jackson Laboratory strain #028864); VIP-cre listed

as B6J.Cg-Vip^{tm1(cre)Zjh}/AreckJ (Jackson Laboratory strain #031628); TdTom listed as B6.Cg-Gt(ROSA)26Sor^{tm14(CAG-tdTomato)Hze}/J (Jackson Laboratory stock #007909); G42 transgenic listed as CB6-Tg(Gad1-EGFP)G42Zjh/J (Jackson Laboratory strain #007677); *Tcf4*^{+/tr} listed as B6;129-*Tcf4*^{tm1Zhu}/J (Jackson Laboratory stock #013598). Mouse colonies were backcrossed for at least six generations in the C57/B6 background, maintained by The Lieber Institute for Brain Development's Animal Facility on a 12-h light/dark cycle and fed ad libitum. *Tcf4*^{+/tr} mouse samples were matched with samples from *Tcf4*^{+/+} (WT) littermates, and sex was randomly selected in each genotype and age group. All procedures were performed in accordance with the National Institutes of Health Guide for the Care and Use of Laboratory Animals and approved by the Johns Hopkins University School of Medicine's Institutional Animal Care and Use Committee.

RNA isolation and qPCR

Total RNA was extracted as previously described [6, 85, 86]. In brief, adult cortices or embryonic (E13.5) ventral forebrain were dissected and homogenized using Trizol. Total RNA was extracted using phenol:chloroform isolation following purification using RNeasy Mini Prep Kit (Qiagen 74004). Following that, complementary DNA (cDNA) was prepared using SuperScriptIII. qPCR assays were carried out in duplicate or triplicate using the QuantStudio3 Real-Time PCR system (Applied Biosystems). qPCR was performed according to the manufacturer's instructions using the Taqman probes (Supplementary Table 6).

Immunohistochemistry

Animals (postnatal day 28–56) are anesthetized with isoflurane and cardio perfused with cold PBS followed by 4% paraformaldehyde (4% PFA). Brains were carefully dissected out and postfixed in 4% PFA overnight before transferring to PBS with 0.1% sodium azide for long term preservation. To cryo protect tissue before frozen sectioning, brains were transferred to 30% sucrose/PBS until fully sank. Frozen sections were sliced to a thickness of 40 μ m for adult brains and 30 μ m for embryonic brains using the Leica sliding microtome. Sections were either mounted on glass slides or free floating for antibody staining. Sections were first washed with PBS three times, 5 min for each wash followed by permeabilization with 0.3% Triton/PBS for 10 min. Sections were washed by PBS and then blocked with 5% BSA in 0.3% Triton/PBS for 1 h at room temperature. Primary antibody was diluted in 0.1% Triton/3% BSA/PBS and incubated at 4 degrees overnight. The following day, slices were washed three times with PBS and incubated with secondary antibodies at room temperature for 2 h and followed by PBS wash before counterstain with DAPI (InvitrogenTM, D1306). Details of primary and secondary antibodies are found in Supplementary Table 7.

Electrophysiology

Animals (postnatal day 28–42) were anesthetized by isoflurane before sacrifice. Brains were quickly dissected out and maintained in ice-cold slicing ACSF containing 75 NaCl, 25 NaHCO₃, 1.25 NaH₂PO₄, 3 KCl, 20 Glucose, 72 Sucrose, 0.5 CaCl₂, and 1 MgCl₂ (in mM) equilibrated with 95% O₂ and 5% CO₂. Acute slices were made using the Leica VT1000 s vibratome with a thickness of 300 μ m. Specimens were first kept at 32 °C

for an hour and transferred and maintained at RT. Whole-cell patch clamp was conducted using an external solution that consists of 125 NaCl, 25 NaHCO₃, 1.25 NaH₂PO₄, 3 KCl, 20 Glucose, 2 CaCl₂, and 1 MgCl₂ (in mM). The internal solution for sEPSC recording is made of 125 KGluconate, 10 KCl, 10 HEPES, 0.1 EGTA, 4 MgATP, 0.3 Na-GTP, 10 Phosphocreatine, and for sIPSC recordings the internal solutions contains 125 KCl, 10 HEPES, 0.1 EGTA, 4 MgATP, 0.3 Na-GTP, 10 Phosphocreatine pH 7.35 with osmolarity around 285–290. In experiments where mEPSC and mIPSC were recorded from the same cell the internal solution is made of the following components: 120 Csmethanesulfonate, 10 CsCl, 10 HEPES, 1 EGTA, 5 QX-314 bromide, 0.1 Spermine, 4 MgATP, 0.3 Na-GTP, 10 Phosphocreatine. mEPSC was acquired while holding cells at –70 mV and mIPSC traces were recorded while holding at 0 mV. Patch pipettes were fabricated from borosilicate glass (N15A; King Precision Glass) to a resistance of 2 to 5 Mohm. Current signals were recorded with either a Multiclamp 700 A amplifier (Molecular Devices) or an Axopatch 200 B amplifier (Molecular Devices) and were filtered at 2 kHz using a built in Bessel filter and digitized at 10 kHz. Voltage signals were filtered at 2 kHz and digitized at 10 kHz. Data was acquired using Axograph software on a Dell PC.

Image acquisition

Visualization was carried out on a Zeiss LSM700, Zeiss Apotome, and BioTek Cytation C10 imager respectively. Imaging and quantification were performed blind to genotypes and conditions.

RNA sequencing analysis

Embryonic mouse brain analysis.—RNA-seq data analysis was executed as previously described [6]. Briefly, reads were aligned to the mm39 mouse genome with the splice-read mapper HISAT2 (version 2.2.1): [`'hisat2-align-s -p 4 -x $GRCm39index --1 $FP --2 $RP -S $SAM --rna-strandness RF -- phred33'`]. Gene expression levels were calculated with the featureCounts tool (version 2.0.1) based on the GENCODE version M30 annotations of the mm39 genome. *Tcf4^{+/tr}* expression was summarized with featureCounts arguments for reversely stranded read pairs: [`'featureCounts -s 2 -p -T 4 -a $GTF -o $OUT $BAM'`]. Differential expression was determined using the R package DESeq2 using raw gene counts to determine DEGs by genotype with the linear model `geneCounts ~ genotype`. Weakly expressed genes (those with an average normalized count <10 across all samples) were dropped from differential expression. The *P* values were adjusted for multiple testing through DESeq2 with a target $\alpha = 0.05$, and mouse genes were considered DEGs at $FDR < 0.05$. We found enriched gene pathways in GO databases with the R package clusterProfiler. The clusterProfiler analysis tested the DEGs at $P < 0.005$. DEGs were separated by positive and negative log₂ fold change. We defined the background as the list of expressed genes with mean normalized counts greater than ten and adjusted for multiple testing with $q < 0.05$.

Mouse cortex and hippocampus scRNA-seq reprocessing.—We downloaded the Allen Institute for Brain Science annotated single cell RNA-seq dataset of the mouse isocortex and hippocampus (<https://portal.brain-map.org/atlas-and-data/rnaseq>, accessed May 2020) [21, 87]. We excluded cells that were reported as low quality or doublets,

class_label = 'Exclude'. We reprocessed counts within R 3.6.3 normalized raw counts for each cell using Seurat v3's SCTransform function [88, 89], and used Scran v1.14.6's findMarkers function to identify marker genes for each cell subtype (subclass_label) that are upregulated for each mouse transcriptionally-defined cell types with respect to all other cell types: test.type = 't', direction = "up", pval.type = "all", groups = "subclass_label". We plot the normalized *Tcf4* expression of each inhibitory neuron subtype in Fig. 1C.

Cell type specific expression analysis (CSEA).—We investigated whether differentially expressed genes (DEGs) in mouse models of PTHS with TCF4 heterozygous mutations were enriched for marker genes of neuronal subtypes defined above [6]. For this cell type-specific expression analysis, we subset to marker genes with a combined false-discovery rate (FDR) less than 0.05. The list of these marker genes are available at the corresponding github repository in the file [AllenMouse_markerGenes_UpInAllPairwise.xlsx](#). We tested the overlap enrichment of up-regulated or down-regulated DEGs measured in TCF4 mutants with marker genes of each Allen transcriptomic subtype with Fisher's Exact tests with a background gene set of all genes expressed in either datasets. We used FDR to correct for multiple hypothesis testing and defined significant enrichment with FDR <0.05 with a positive odds ratio (OR > 1). The numerical results of DEGs are reported in Supplementary Table 5 and at the corresponding github repository in the file [overlapDEG_FisherEnrichment_plot_AllenMarkerGenesAllGroups.xlsx](#). We plot the CSEA enrichments of PTHS DEGs by mouse cell subtypes in Fig. 1A.

Bulk PTHS mouse brain RNA-seq deconvolution.—We investigated whether the estimated proportion of neuronal subtypes shifted in TCF4 mutants bulk RNA-seq profiles using cellular deconvolution as described previously [90]. We create the reference cell type expression profile using the SCTransform expression levels in the marker genes [Mouse cortex and hippocampus scRNA-seq reprocessing](#). We deconvolve Phan, Bohlen et al. samples with this reference to estimate the proportion of each cell subtype present within each bulk RNA-seq profile. We tested the difference in cell type proportion by genotype while adjusting for the following covariates with a linear regression as in Phan, Bohlen et al: Proportion ~ Genotype + Line + Age. We adjusted the p-value in difference between genotypes for each cell subtype proportions with FDR for multiple cell type hypotheses and reported significant changes for cell types with FDR < 0.05, Fig. 1B.

Discovery of candidate TCF4 co-binding transcription factors.—We downloaded raw sequencing files from three published datasets of TCF4 ChIP-seq in SH-SY55 or the related SK-N-SH cell line under accession codes (GEO GSE96915, GEO GSE112704, ENCODE ENCSR922RFY) [29–31]. We followed the ENCODE ChIP-seq data processing pipeline (<https://github.com/ENCODE-DCC/chip-seq-pipeline2>) v2.2.1 with default parameters to align the data by project and call peaks [91]. Subsequently, we used the optimal reproducible peaks from each dataset to predict which TF are bound at TCF4 ChIP-seq using the computational method, WhichTF v0.2 with default parameters [92]. Unfortunately, TCF4 is not a TF that is part of this repository. We combined predicted bound TF across the 3 datasets for TFs that were significantly enriched in TCF4 ChIP-seq peaks

with $FDR < 0.05$ and report the highest FDR across any dataset for each TF, as well as how many datasets that TF was significant in.

To assess the potential co-regulation of these candidate co-bound TF, we downloaded a human postmortem prefrontal cortex single nuclei RNA-seq dataset [32]. Due to the sparsity of genes in single cell data, especially in weakly expressed transcription factors, we imputed expression using the `SeuratWrappers::RunALRA()` function [93]. We plot the imputed expression of *TCF4* and each expressed candidate co-binding transcription factor and calculate the Pearson correlation with *TCF4* in the subset of the subjects >14 years old to match the developmental stages of the animals in our study. We additionally assessed if these transcription factors were reported by the original authors as developmentally-regulated across cortical cell types (<https://perkinsinstitute.shinyapps.io/listerlab-pfc-major-trends/>) and report those that are developmentally regulated in cortical INs.

Statistical Analysis

GraphPad Prism (GraphPad Software, San Diego, CA) was used to conduct statistical analyses for all experiments. Results are presented as mean \pm SEM unless otherwise stated in figure legends. All data sets were tested for normality using D'Agostino Pearson omnibus normality test. When comparing two normally distributed groups, unpaired Student's *t*-test was performed. The non-parametric Mann–Whitney test was used when the datasets were not normally distributed. For multiple comparison testing of the AP input-output curves, 2-way ANOVA was performed. A *p* value of less than 0.05 was considered statistically. Significance was indicated as follows: **p* < 0.05, ***p* < 0.01, ****p* < 0.001. All data was acquired from three or more mice across multiple litters.

Supplementary Material

Refer to Web version on PubMed Central for supplementary material.

ACKNOWLEDGEMENTS

We are grateful for the vision and generosity of the Lieber and Maltz families, who made this work possible. We thank Dr. Keri Martinowich for sharing the CST-cre and TdTom mouse lines. This work was supported by the Lieber Institute, the Pitt-Hopkins Research Foundation Award (BJM), and a NIMH grant R01MH110487 (BJM). The content is solely the responsibility of the authors and does not necessarily represent the official views of the National Institutes of Health.

DATA AVAILABILITY

Code for RNA-seq analyses in this study are available online at https://github.com/LieberInstitute/PTHS_interneurons. No new genomic sequencing experiments were performed in this study.

REFERENCES

1. Teixeira JR, Szeto RA, Carvalho VMA, Muotri AR, Papes F. Transcription factor 4 and its association with psychiatric disorders. *Transl Psychiatry*. 2021;11:19. [PubMed: 33414364]
2. Chen H-Y, Bohlen JF, Maher BJ. Molecular and cellular function of transcription Factor 4 in Pitt-Hopkins syndrome. *Dev Neurosci*. 2021;43:159–67. [PubMed: 34134113]

3. de Winter CF, Baas M, Bijlsma EK, van Heukelingen J, Routledge S, Hennekam RCM. Phenotype and natural history in 101 individuals with Pitt-Hopkins syndrome through an internet questionnaire system. *Orphanet J Rare Dis.* 2016;11:37. [PubMed: 27072915]
4. Zollino M, Zweier C, Van Balkom ID, Sweetser DA, Alaimo J, Bijlsma EK, et al. Diagnosis and management in Pitt-Hopkins syndrome: first international consensus statement. *Clin Genet.* 2019;95:462–78. [PubMed: 30677142]
5. Rannals MD, Hamersky GR, Page SC, Campbell MN, Briley A, Gallo RA, et al. Psychiatric risk gene transcription factor 4 regulates intrinsic excitability of prefrontal neurons via repression of *scn10a* and *KCNQ1*. *Neuron.* 2016;90:43–55. [PubMed: 26971948]
6. Phan BN, Bohlen JF, Davis BA, Ye Z, Chen H-Y, Mayfield B, et al. A myelin-related transcriptomic profile is shared by Pitt-Hopkins syndrome models and human autism spectrum disorder. *Nat Neurosci.* 2020;23:375–85. [PubMed: 32015540]
7. Kim H, Berens NC, Ochandarena NE, Philpot BD. Region and cell type distribution of TCF4 in the postnatal mouse brain. *Front Neuroanat.* 2020;14:42. [PubMed: 32765228]
8. Ling JP, Wilks C, Charles R, Leavey PJ, Ghosh D, Jiang L, et al. ASCOT identifies key regulators of neuronal subtype-specific splicing. *Nat Commun.* 2020;11:137. [PubMed: 31919425]
9. Tasic B, Menon V, Nguyen TN, Kim TK, Jarsky T, Yao Z, et al. Adult mouse cortical cell taxonomy revealed by single cell transcriptomics. *Nat Neurosci.* 2016;19:335–46. [PubMed: 26727548]
10. Roux L, Buzsáki G. Tasks for inhibitory interneurons in intact brain circuits. *Neuropharmacology.* 2015;88:10–23. [PubMed: 25239808]
11. Marín O. Interneuron dysfunction in psychiatric disorders. *Nat Rev Neurosci.* 2012;13:107–20. [PubMed: 22251963]
12. Nelson SB, Valakh V. Excitatory/inhibitory balance and circuit homeostasis in autism spectrum disorders. *Neuron.* 2015;87:684–98. [PubMed: 26291155]
13. Scharfman HE. The neurobiology of epilepsy. *Curr Neurol Neurosci Rep.* 2007;7:348–54. [PubMed: 17618543]
14. Uhlhaas PJ, Singer W. Abnormal neural oscillations and synchrony in schizophrenia. *Nat Rev Neurosci.* 2010;11:100–13. [PubMed: 20087360]
15. Fishell G, Kepecs A. Interneuron types as attractors and controllers. *Annu Rev Neurosci.* 2020;43:1–30. [PubMed: 31299170]
16. Tremblay R, Lee S, Rudy B. Gabaergic interneurons in the neocortex: from cellular properties to circuits. *Neuron.* 2016;91:260–92. [PubMed: 27477017]
17. Sultan KT, Shi S-H Generation of diverse cortical inhibitory interneurons. *Wiley Interdiscip Rev Dev Biol.* 2018; 7. 10.1002/wdev.306.
18. de Lecea L, del Rio JA, Criado JR, Alcántara S, Morales M, Danielson PE, et al. Cortistatin is expressed in a distinct subset of cortical interneurons. *J Neurosci.* 1997;17:5868–80. [PubMed: 9221784]
19. Hébert JM, Fishell G. The genetics of early telencephalon patterning: some assembly required. *Nat Rev Neurosci.* 2008;9:678–85. [PubMed: 19143049]
20. Thompson CL, Ng L, Menon V, Martinez S, Lee C-K, Glattfelder K, et al. A high-resolution spatiotemporal atlas of gene expression of the developing mouse brain. *Neuron.* 2014;83:309–23. [PubMed: 24952961]
21. Yao Z, van Velthoven CTJ, Nguyen TN, Goldy J, Seden-Cortes AE, Baftizadeh F, et al. A taxonomy of transcriptomic cell types across the isocortex and hippocampal formation. *Cell.* 2021;184:3222–3241.e26. [PubMed: 34004146]
22. Koopmans F, van Nierop P, Andres-Alonso M, Byrnes A, Cijssouw T, Coba MP, et al. SynGO: an evidence-based, expert-curated knowledge base for the synapse. *Neuron.* 2019;103:217–234.e4. [PubMed: 31171447]
23. Bertrand N, Castro DS, Guillemot F. Proneural genes and the specification of neural cell types. *Nat Rev Neurosci.* 2002;3:517–30. [PubMed: 12094208]
24. Moen MJ, Adams HHH, Brandsma JH, Dekkers DHW, Akinci U, Karkampouna S, et al. An interaction network of mental disorder proteins in neural stem cells. *Transl Psychiatry.* 2017;7:e1082. [PubMed: 28375211]

25. Wittmann M-T, Katada S, Sock E, Kirchner P, Ekici AB, Wegner M et al. scRNA sequencing uncovers a TCF4-dependent transcription factor network regulating commissure development in mouse. *Development*. 2021; 148. 10.1242/dev.196022.
26. Wang Y, Liu L, Lin M. Psychiatric risk gene transcription factor 4 preferentially regulates cortical interneuron neurogenesis during early brain development. *J Biomed Res*. 2022;36:242–54. [PubMed: 35965434]
27. Ravasi T, Suzuki H, Cannistraci CV, Katayama S, Bajic VB, Tan K, et al. An atlas of combinatorial transcriptional regulation in mouse and man. *Cell*. 2010;140:744–52. [PubMed: 20211142]
28. Fedorova E, Zink D. Nuclear architecture and gene regulation. *Biochim Biophys Acta*. 2008;1783:2174–84. [PubMed: 18718493]
29. Xia H, Jahr FM, Kim N-K, Xie L, Shabalin AA, Bryois J. Building a schizophrenia genetic network: transcription factor 4 regulates genes involved in neuronal development and schizophrenia risk. *Hum Mol Genet*. 2018;27:3246–56. [PubMed: 29905862]
30. ENCODE Project Consortium. An integrated encyclopedia of DNA elements in the human genome. *Nature*. 2012;489:57–74. [PubMed: 22955616]
31. Forrest MP, Hill MJ, Kavanagh DH, Tansey KE, Waite AJ, Blake DJ. The psychiatric risk gene transcription factor 4 (TCF4) regulates neurodevelopmental pathways associated with schizophrenia, autism, and intellectual disability. *Schizophr Bull*. 2018;44:1100–10. [PubMed: 29228394]
32. Herring CA, Simmons RK, Freytag S, Poppe D, Moffet JJD, Pflueger J, et al. Human prefrontal cortex gene regulatory dynamics from gestation to adulthood at single-cell resolution. *Cell*. 2022;185:4428–4447.e28. [PubMed: 36318921]
33. Wedel M, Fröb F, Elsesser O, Wittmann M-T, Lie DC, Reis A, et al. Transcription factor Tcf4 is the preferred heterodimerization partner for Olig2 in oligodendrocytes and required for differentiation. *Nucleic Acids Res*. 2020;48:4839–57. [PubMed: 32266943]
34. Sepp M, Vihma H, Nurm K, Urb M, Page SC, Roots K, et al. The intellectual disability and schizophrenia associated transcription factor TCF4 is regulated by neuronal activity and protein kinase A. *J Neurosci*. 2017;37:10516–27. [PubMed: 28951451]
35. Nurm K, Sepp M, Castany-Pladevall C, Creus-Muncunill J, Tuvikene J, Sirp A et al. Isoform-specific reduction of the basic helix-loop-helix transcription factor TCF4 levels in Huntington's Disease. *eNeuro*. 2021; 8. 10.1523/ENEURO.0197-21.2021.
36. Fode C, Ma Q, Casarosa S, Ang SL, Anderson DJ, Guillemot F. A role for neural determination genes in specifying the dorsoventral identity of telencephalic neurons. *Genes Dev*. 2000;14:67–80. [PubMed: 10640277]
37. Parras CM, Schuurmans C, Scardigli R, Kim J, Anderson DJ, Guillemot F. Divergent functions of the proneural genes Mash1 and Ngn2 in the specification of neuronal subtype identity. *Genes Dev*. 2002;16:324–38. [PubMed: 11825874]
38. Marin O, Anderson SA, Rubenstein JL. Origin and molecular specification of striatal interneurons. *J Neurosci*. 2000;20:6063–76. [PubMed: 10934256]
39. Allaway KC, Machold R. Developmental specification of forebrain cholinergic neurons. *Dev Biol*. 2017;421:1–7. [PubMed: 27847324]
40. Tang K, Rubenstein JLR, Tsai SY, Tsai M-J. COUP-TFII controls amygdala patterning by regulating neuropilin expression. *Development*. 2012;139:1630–9. [PubMed: 22492355]
41. Bandler RC, Mayer C. Deciphering inhibitory neuron development: the paths to diversity. *Curr Opin Neurobiol*. 2023;79:102691. [PubMed: 36805715]
42. Gupta A, Wang Y, Markram H. Organizing principles for a diversity of GABAergic interneurons and synapses in the neocortex. *Science*. 2000;287:273–8. [PubMed: 10634775]
43. Jiang X, Shen S, Cadwell CR, Berens P, Sinz F, Ecker AS, et al. Principles of connectivity among morphologically defined cell types in adult neocortex. *Science*. 2015;350:aac9462. [PubMed: 26612957]
44. Pfeffer CK, Xue M, He M, Huang ZJ, Scanziani M. Inhibition of inhibition in visual cortex: the logic of connections between molecularly distinct interneurons. *Nat Neurosci*. 2013;16:1068–76. [PubMed: 23817549]

45. Lee S, Kruglikov I, Huang ZJ, Fishell G, Rudy B. A disinhibitory circuit mediates motor integration in the somatosensory cortex. *Nat Neurosci.* 2013;16:1662–70. [PubMed: 24097044]
46. Pi H-J, Hangya B, Kvitsiani D, Sanders JI, Huang ZJ, Kepecs A. Cortical interneurons that specialize in disinhibitory control. *Nature.* 2013;503:521–4. [PubMed: 24097352]
47. Campagnola L, Seeman SC, Chartrand T, Kim L, Hoggarth A, Gamlin C, et al. Local connectivity and synaptic dynamics in mouse and human neocortex. *Science.* 2022;375:eabj5861. [PubMed: 35271334]
48. Ferrante M, Tahvildari B, Duque A, Hadzipasic M, Salkoff D, Zaghera EW, et al. Distinct functional groups emerge from the intrinsic properties of molecularly identified entorhinal interneurons and principal cells. *Cereb Cortex.* 2017;27:3186–207. [PubMed: 27269961]
49. Davis BA, Chen H-Y, Ye Z, Ostlund I, Tippiani M, Das D, et al. TCF4 mutations disrupt synaptic function through dysregulation of RIMBP2 in patient-derived cortical neurons. *Biol Psychiatry.* 2023. 10.1016/j.biopsych.2023.07.021.
50. Papes F, Camargo AP, de Souza JS, Carvalho VMA, Szeto RA, LaMontagne E, et al. Transcription Factor 4 loss-of-function is associated with deficits in progenitor proliferation and cortical neuron content. *Nat Commun.* 2022;13:2387. [PubMed: 35501322]
51. Cleary CM, James S, Maher BJ, Mulkey DK. Disordered breathing in a Pitt-Hopkins syndrome model involves Phox2b-expressing parafacial neurons and aberrant Nav1.8 expression. *Nat Commun.* 2021;12:5962. [PubMed: 34645823]
52. Li H, Zhu Y, Morozov YM, Chen X, Page SC, Rannals MD, et al. Disruption of TCF4 regulatory networks leads to abnormal cortical development and mental disabilities. *Mol Psychiatry.* 2019;24:1235–46. [PubMed: 30705426]
53. Rubenstein JLR, Merzenich MM. Model of autism: increased ratio of excitation/inhibition in key neural systems. *Genes Brain Behav.* 2003;2:255–67. [PubMed: 14606691]
54. Anderson S, Mione M, Yun K, Rubenstein JL. Differential origins of neocortical projection and local circuit neurons: role of Dlx genes in neocortical interneuronogenesis. *Cereb Cortex.* 1999;9:646–54. [PubMed: 10498283]
55. Wamsley B, Fishell G. Genetic and activity-dependent mechanisms underlying interneuron diversity. *Nat Rev Neurosci.* 2017;18:299–309. [PubMed: 28381833]
56. Southwell DG, Paredes MF, Galvao RP, Jones DL, Froemke RC, Sebe JY, et al. Intrinsically determined cell death of developing cortical interneurons. *Nature.* 2012;491:109–13. [PubMed: 23041929]
57. Zhang Y, Cai Z, Hu G, Hu S, Wang Y, Li N, et al. Transcription factor 4 controls positioning of cortical projection neurons through regulation of cell adhesion. *Mol Psychiatry.* 2021;26:6562–77. [PubMed: 33963287]
58. Braun K, Häberle BM, Wittmann M-T, Lie DC. Enriched environment ameliorates adult hippocampal neurogenesis deficits in Tcf4 haploinsufficient mice. *BMC Neurosci.* 2020;21:50. [PubMed: 33228529]
59. Mesman S, Bakker R, Smidt MP. Tcf4 is required for correct brain development during embryogenesis. *Mol Cell Neurosci.* 2020;106:103502. [PubMed: 32474139]
60. Schoof M, Hellwig M, Harrison L, Holdhof D, Lauffer MC, Niesen J, et al. The basic helix-loop-helix transcription factor TCF4 impacts brain architecture as well as neuronal morphology and differentiation. *Eur J Neurosci.* 2020;51:2219–35. [PubMed: 31919899]
61. Chen T, Wu Q, Zhang Y, Lu T, Yue W, Zhang D. Tcf4 controls neuronal migration of the cerebral cortex through regulation of Bmp7. *Front Mol Neurosci.* 2016;9:94. [PubMed: 27752241]
62. Forrest MP, Waite AJ, Martin-Rendon E, Blake DJ. Knockdown of human TCF4 affects multiple signaling pathways involved in cell survival, epithelial to mesenchymal transition and neuronal differentiation. *PLoS One.* 2013;8:e73169. [PubMed: 24058414]
63. Page SC, Hamersky GR, Gallo RA, Rannals MD, Calcaterra NE, Campbell MN, et al. The schizophrenia- and autism-associated gene, transcription factor 4 regulates the columnar distribution of layer 2/3 prefrontal pyramidal neurons in an activity-dependent manner. *Mol Psychiatry.* 2018;23:304–15. [PubMed: 28289282]

64. Weissman TA, Riquelme PA, Ivic L, Flint AC, Kriegstein AR. Calcium waves propagate through radial glial cells and modulate proliferation in the developing neocortex. *Neuron*. 2004;43:647–61. [PubMed: 15339647]
65. LoTurco JJ, Owens DF, Heath MJ, Davis MB, Kriegstein AR. GABA and glutamate depolarize cortical progenitor cells and inhibit DNA synthesis. *Neuron*. 1995;15:1287–98. [PubMed: 8845153]
66. Owens DF, Flint AC, Dammerman RS, Kriegstein AR. Calcium dynamics of neocortical ventricular zone cells. *Dev Neurosci*. 2000;22:25–33. [PubMed: 10657695]
67. Manent J-B, Demarque M, Jorquera I, Pellegrino C, Ben-Ari Y, Aniksztejn L, et al. A noncanonical release of GABA and glutamate modulates neuronal migration. *J Neurosci*. 2005;25:4755–65. [PubMed: 15888651]
68. Lawler AJ, Brown AR, Bouchard RS, Toong N, Kim Y, Velraj N, et al. Cell type-specific oxidative stress genomic signatures in the globus pallidus of dopamine-depleted mice. *J Neurosci*. 2020;40:9772–83. [PubMed: 33188066]
69. Zhang Y, Cai Y, Wang Y, Deng X, Zhao Y, Zhang Y, et al. Survival control of oligodendrocyte progenitor cells requires the transcription factor 4 during olfactory bulb development. *Cell Death Dis*. 2021;12:91. [PubMed: 33462220]
70. Micheva KD, Wolman D, Mensh BD, Pax E, Buchanan J, Smith SJ et al. A large fraction of neocortical myelin ensheathes axons of local inhibitory neurons. *eLife*. 2016; 5. 10.7554/eLife.15784.
71. Stedehouder J, Couey JJ, Brizee D, Hosseini B, Slotman JA, Dirven CMF, et al. Fast-spiking parvalbumin interneurons are frequently myelinated in the cerebral cortex of mice and humans. *Cereb Cortex*. 2017;27:5001–13. [PubMed: 28922832]
72. Zonouzi M, Berger D, Jokhi V, Kedaigle A, Lichtman J, Arlotta P. Individual oligodendrocytes show bias for inhibitory axons in the neocortex. *Cell Rep*. 2019;27:2799–2808.e3. [PubMed: 31167127]
73. Kessaris N, Fogarty M, Iannarelli P, Grist M, Wegner M, Richardson WD. Competing waves of oligodendrocytes in the forebrain and postnatal elimination of an embryonic lineage. *Nat Neurosci*. 2006;9:173–9. [PubMed: 16388308]
74. Orduz D, Benamer N, Ortolani D, Coppola E, Vigier L, Pierani A, et al. Developmental cell death regulates lineage-related interneuron-oligodendroglia functional clusters and oligodendrocyte homeostasis. *Nat Commun*. 2019;10:4249. [PubMed: 31534164]
75. Kim H, Gao EB, Draper A, Berens NC, Vihma H, Zhang X et al. Rescue of behavioral and electrophysiological phenotypes in a Pitt-Hopkins syndrome mouse model by genetic restoration of Tcf4 expression. *eLife*. 2022; 11. 10.7554/eLife.72290.
76. Chen Y-JJ, Friedman BA, Ha C, Durinck S, Liu J, Rubenstein JL, et al. Single-cell RNA sequencing identifies distinct mouse medial ganglionic eminence cell types. *Sci Rep*. 2017;7:45656. [PubMed: 28361918]
77. Matricardi S, Bonanni P, Iapadre G, Elia M, Cesaroni E, Danieli A, et al. Epilepsy, electroclinical features, and long-term outcomes in Pitt-Hopkins syndrome due to pathogenic variants in the TCF4 gene. *Eur J Neurol*. 2022;29:19–25. [PubMed: 34519126]
78. Bone M, Goodspeed K, Sirsi D. Epilepsy and electroencephalography in Pitt-Hopkins syndrome. *J Transl Genet Genom*. 2022;6:169–78.
79. Martinowich K, Das D, Sripathy SR, Mai Y, Kenney RF, Maher BJ. Evaluation of Nav1.8 as a therapeutic target for Pitt Hopkins Syndrome. *Mol Psychiatry*. 2023;28:76–82. [PubMed: 36224259]
80. Gonzalez-Burgos G, Cho RY, Lewis DA. Alterations in cortical network oscillations and parvalbumin neurons in schizophrenia. *Biol Psychiatry*. 2015;77:1031–40. [PubMed: 25863358]
81. Buzsáki G, Wang X-J. Mechanisms of gamma oscillations. *Annu Rev Neurosci*. 2012;35:203–25. [PubMed: 22443509]
82. Gu B, Shorter JR, Williams LH, Bell TA, Hock P, Dalton KA, et al. Collaborative Cross mice reveal extreme epilepsy phenotypes and genetic loci for seizure susceptibility. *Epilepsia*. 2020;61:2010–21. [PubMed: 32852103]

83. Harris KD, Shepherd GMG. The neocortical circuit: themes and variations. *Nat Neurosci*. 2015;18:170–81. [PubMed: 25622573]
84. Karnani MM, Jackson J, Ayzenshtat I, Tucciarone J, Manoocheri K, Snider WG, et al. Cooperative subnetworks of molecularly similar interneurons in mouse neocortex. *Neuron*. 2016;90:86–100. [PubMed: 27021171]
85. Page SC, Sripathy SR, Farinelli F, Ye Z, Wang Y, Hiler DJ et al. Electrophysiological measures from human iPSC-derived neurons are associated with schizophrenia clinical status and predict individual cognitive performance. *Proc Natl Acad Sci USA*. 2022; 119. 10.1073/pnas.2109395119.
86. Sripathy SR, Wang Y, Moses RL, Fatemi A, Batista DA, Maher BJ. Generation of 10 patient-specific induced pluripotent stem cells (iPSCs) to model Pitt-Hopkins Syndrome. *Stem Cell Res*. 2020;48:102001. [PubMed: 32971458]
87. Tasic B, Yao Z, Graybuck LT, Smith KA, Nguyen TN, Bertagnolli D, et al. Shared and distinct transcriptomic cell types across neocortical areas. *Nature*. 2018;563:72–78. [PubMed: 30382198]
88. Stuart T, Butler A, Hoffman P, Hafemeister C, Papalexi E, Mauck WM, et al. Comprehensive integration of single. *Cell Data*. *Cell*. 2019;177:1888–1902.e21. [PubMed: 31178118]
89. Hafemeister C, Satija R. Normalization and variance stabilization of single-cell RNA-seq data using regularized negative binomial regression. *Genome Biol*. 2019;20:296. [PubMed: 31870423]
90. Chiu Y-J, Hsieh Y-H, Huang Y-H. Improved cell composition deconvolution method of bulk gene expression profiles to quantify subsets of immune cells. *BMC Med Genomics*. 2019;12:169. [PubMed: 31856824]
91. Landt SG, Marinov GK, Kundaje A, Kheradpour P, Pauli F, Batzoglou S, et al. ChIP-seq guidelines and practices of the ENCODE and modENCODE consortia. *Genome Res*. 2012;22:1813–31. [PubMed: 22955991]
92. Tanigawa Y, Dyer ES, Bejerano G. WhichTF is functionally important in your open chromatin data? *PLoS Comput Biol*. 2022;18:e1010378. [PubMed: 36040971]
93. Linderman GC, Zhao J, Roulis M, Bielecki P, Flavell RA, Nadler B, et al. Zero-preserving imputation of single-cell RNA-seq data. *Nat Commun*. 2022;13:192. [PubMed: 35017482]

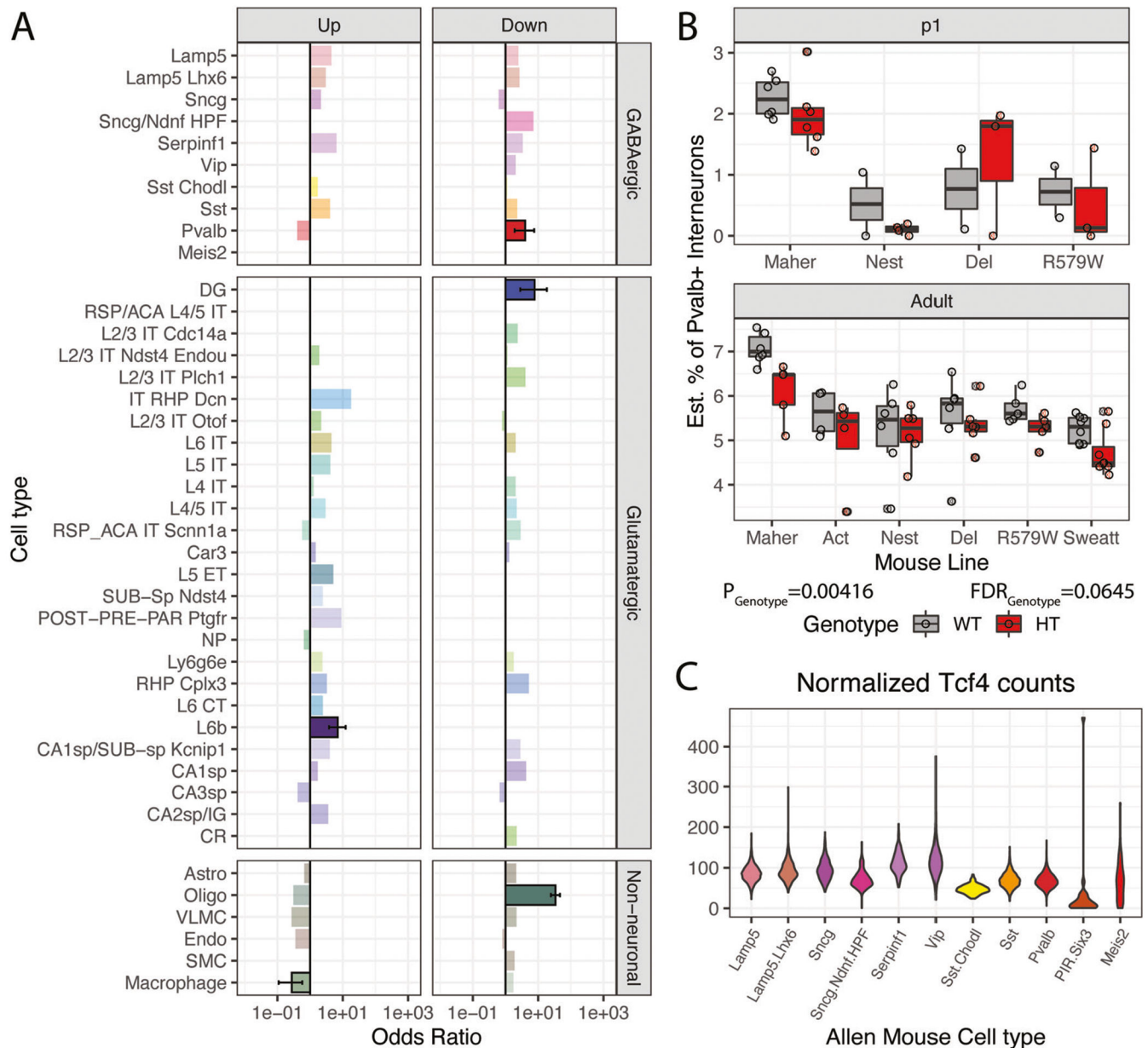


Fig. 1. Cell type-specific expression analyses and cellular deconvolution of bulk RNA-seq data predicts a reduction in PV + INs in *Tcf4*^{+/-mut} mice.

A. Bar plot showing the odds ratio (\pm S.E.M) from gene set enrichment analyses of up- or down-regulated genes in *Tcf4*^{+/-mut} mice with marker genes for mouse cell types identified by single cell RNA-seq. Statistically significant enrichments at FDR < 0.05 are plotted with bold-black outlines. The full numerical results are reported in Supplementary Table 5. B. Cellular deconvolution of *Tcf4*^{+/-mut} across different models of *Tcf4* mutations estimates a decrease in PV+ INs in mutant mice. The *p*-value and FDR are reported for the overall effect of *Tcf4* mutation across mouse lines and ages. C. Violin plots of normalized *Tcf4* expression in the Allen Brain Atlas mouse single cell RNA-seq of interneuron types.

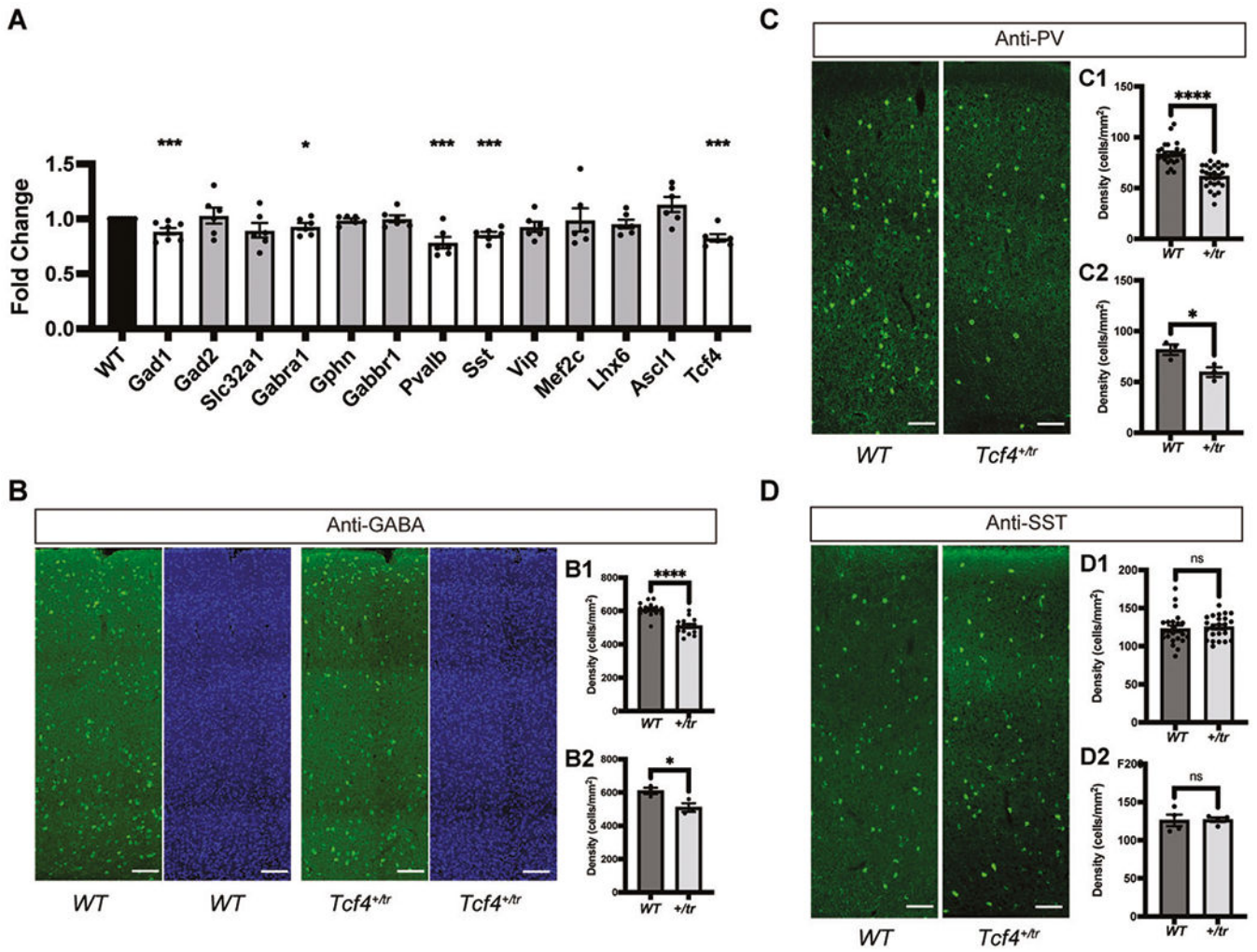


Fig. 2. Dysregulation of IN specific gene expression in the PTHS mouse model.

A qPCR of IN-specific gene expression in the adult cortex of WT and *Tcf4*^{+/-} mice. Expression of *Gad1* ($p = 0.000678$), *Gabra1* ($p = 0.01514$), *Pvalb* ($p = 0.002031$), *Sst* ($p = 0.000191$), and *Tcf4* ($p = 0.000537$) was downregulated in the *Tcf4*^{+/-} mice compared to WT littermates. **B** IHC staining of GABA (green) and DAPI (blue) in the adult somatosensory cortex of WT (left) and *Tcf4*^{+/-} (right) littermates. The density of GABA+ cells was reduced in *Tcf4*^{+/-} mice (**B1** WT 609.8 ± 10.55, $N = 15$ sections, *Tcf4*^{+/-} 509.5 ± 12.19, $N = 15$ sections, $p < 0.0001$; **B2** WT 609.8 ± 18.83, $N = 3$ animals, *Tcf4*^{+/-} 509.5 ± 25.89, $N = 3$ animals, $p = 0.0351$). **C** IHC staining of PV+ cells in the adult somatosensory cortex of WT (left) and *Tcf4*^{+/-} (right) littermates. The density of PV+ cells was reduced in *Tcf4*^{+/-} mice (**C1** WT 83.54 ± 2.16, $N = 26$ sections, *Tcf4*^{+/-} 61.46 ± 2.2, $N = 26$ sections, $p < 0.0001$; **C2** WT 81.7 ± 5.14, $N = 3$ animals, *Tcf4*^{+/-} 59.61 ± 4.72, $N = 3$ animals, $p = 0.0341$). **D** IHC staining of SST+ cells in the adult somatosensory cortex of WT (left) and *Tcf4*^{+/-} (right) littermates. The density of SST+ cells was not different between genotypes (**D1** WT 122.7 ± 4.29, $N = 23$ sections, *Tcf4*^{+/-} 125.3 ± 3.18, $N = 23$ sections, $p = 0.6386$; **D2** WT 126 ± 7.61, $N = 4$ animals, *Tcf4*^{+/-} 126.9 ± 3.0, $N = 4$ animals, $p = 0.9125$). Stats presented as mean ± s.e.m, scale bars = 100 μ m.

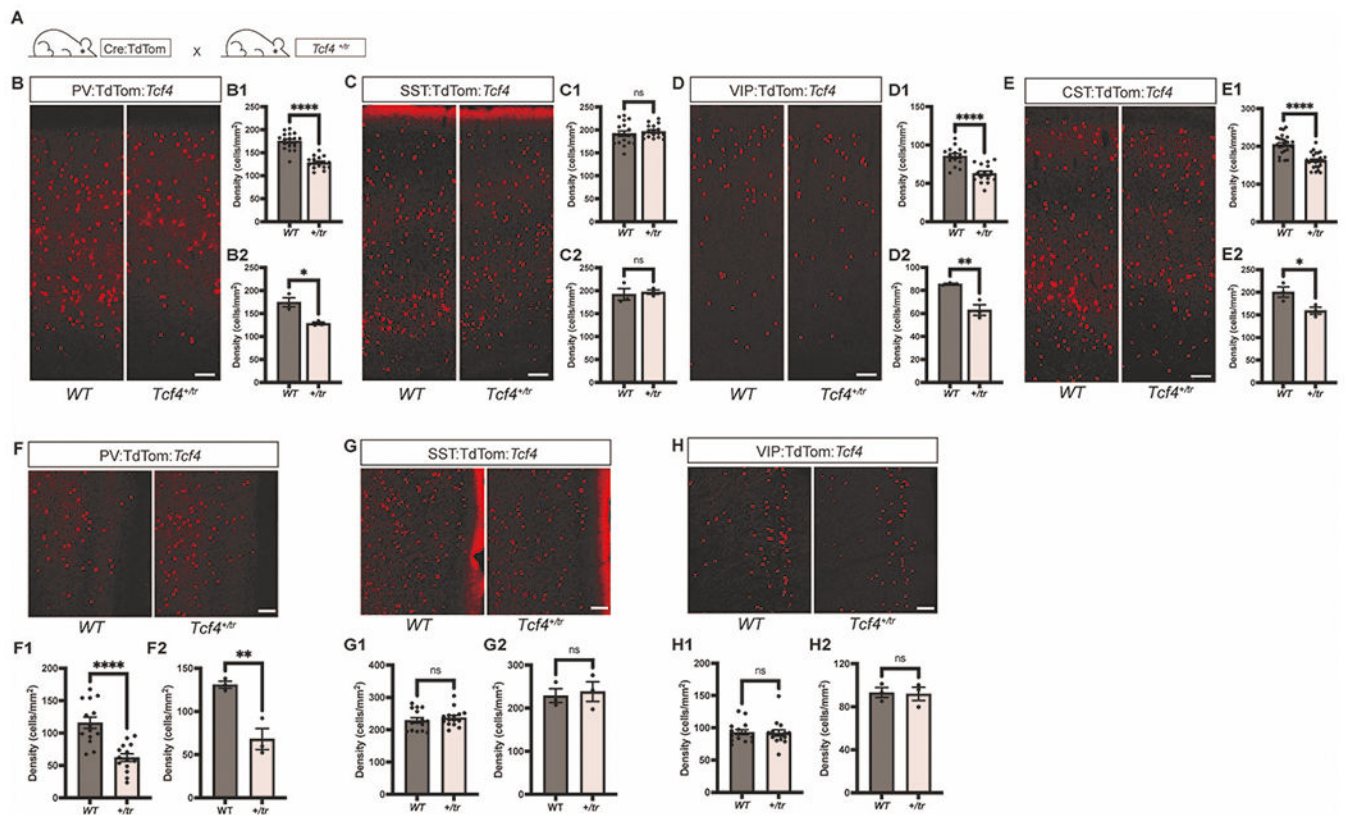


Fig. 3. Reduced density of specific subclasses of INs in the PTHS mouse cortex.

A Schematic design of Cre-dependent labeling of various cortical interneuron subclasses. **B** The density of PV+ INs was reduced in the somatosensory cortex of *Tcf4^{+/-}* mice (**B1** WT 175.3 ± 4.55, *N* = 17 sections, *Tcf4^{+/-}* 128.5 ± 3.08, *N* = 17 sections, *p* < 0.0001; **B2** WT 174.4 ± 9.76, *N* = 3 animals, *Tcf4^{+/-}* 128.4 ± 2.92, *N* = 3 animals, *p* = 0.0107). **C** No effect of *Tcf4* loss-of-function on the density of SST+ INs in the somatosensory cortex of *Tcf4^{+/-}* mice (**C1** WT 192.1 ± 5.74, *N* = 18 sections, *Tcf4^{+/-}* 196.8 ± 3.4, *N* = 17 sections, *p* = 0.496; **C2** WT 192.1 ± 12.72, *N* = 3 animals, *Tcf4^{+/-}* 197.3 ± 4.8, *N* = 3 animals, *p* = 0.725). **D** The density of VIP+ INs was reduced in the somatosensory cortex of *Tcf4^{+/-}* mice (**D1**. WT 85.6 ± 3.17, *N* = 15 sections, *Tcf4^{+/-}* 62.92 ± 3.11, *N* = 15 sections, *p* < 0.0001; **D2** WT 85.6 ± 0.59, *N* = 3 animals, *Tcf4^{+/-}* 62.92 ± 4.64, *N* = 3 animals *p* = 0.0083). **E** The density of CST+ INs was reduced in the somatosensory cortex of *Tcf4^{+/-}* mice (**E1** WT 205 ± 4.79, *N* = 26 sections, *Tcf4^{+/-}* 162.5 ± 3.92, *N* = 26 sections, *p* < 0.0001; **E2** WT 200.6 ± 11.61, *N* = 3 animals *Tcf4^{+/-}* 159.4 ± 7.72, *N* = 3 animals, *p* = 0.0419). **F** The density of PV+ INs was reduced in the medial prefrontal cortex of *Tcf4^{+/-}* mice (**F1** WT 115.9 ± 8.84, *N* = 14 sections, *Tcf4^{+/-}* 62 ± 5.86, *N* = 14 sections, *p* < 0.0001; **F2** WT 131 ± 4.11, *N* = 3 animals, *Tcf4^{+/-}* 68.04 ± 12.25, *N* = 3 animals, *p* = 0.0082). **G** The density of SST+ INs was not different in the medial prefrontal cortex of *Tcf4^{+/-}* mice (**G1** WT 229 ± 8.32, *N* = 15 sections, *Tcf4^{+/-}* 237.5 ± 6.97, *N* = 15 sections, *p* = 0.4406; **G2** WT 229 ± 16.2, *N* = 3 animals, *Tcf4^{+/-}* 238.5 ± 22.78, *N* = 3 animals, *p* = 0.7512). **H** The density of VIP+ INs was not different in the medial prefrontal cortex of *Tcf4^{+/-}* mice (**H1** WT 93.17 ± 3.95, *N* = 15 sections, *Tcf4^{+/-}* 87.86 ± 5.01, *N* = 14 sections, *p* = 0.3043; **H2** WT 93.17 ± 4.64, *N* = 3

animals, $Tcf4^{+/tr}$ 87.87 ± 4.64 , $N = 3$ animals, $p = 0.4644$). Stats mean \pm s.e.m., scale bars **B–H** = 100 μm , scale bar in **H** = 30 μm .

Author Manuscript

Author Manuscript

Author Manuscript

Author Manuscript

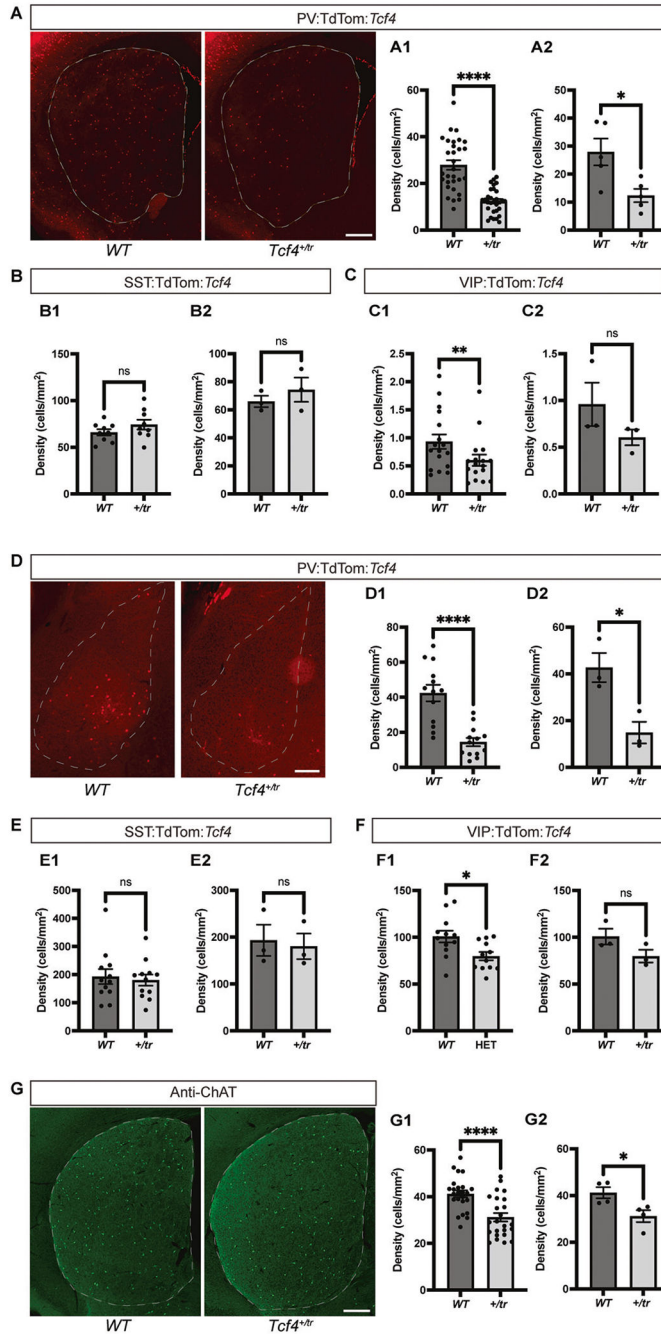


Fig. 4. Reduced density of specific subclasses of INs in subcortical brain regions.

A Representative images showing PV+ INs in the striatum of WT and *Tcf4*^{+/-tr} mice. **A1** The density of PV+ INs was reduced in the striatum of *Tcf4*^{+/-tr} mice (**A1** WT 27.91 ± 2.03 , $N = 30$ sections, HET 12.36 ± 1 , $N = 30$ sections, $p < 0.0001$; **A2** WT 27.91 ± 4.79 , $N = 5$ animals, *Tcf4*^{+/-tr} 12.36 ± 2.37 , $N = 5$ animals, $p = 0.0196$). **B** No effect of *Tcf4* loss-of-function on the density of SST+ INs in the striatum of *Tcf4*^{+/-tr} mice (**B1** WT 65.98 ± 3.35 , $N = 9$ sections, *Tcf4*^{+/-tr} 74.31 ± 5.3 , $N = 9$ sections, $p = 0.2031$; **B2** WT 65.98 ± 4.09 , $N = 3$ animals, *Tcf4*^{+/-tr} 74.31 ± 8.61 , $N = 3$ animals, $p = 0.4318$). **C** The density of VIP+

INs was reduced in the striatum of *Tcf4^{+/-tr}* mice (**C1** WT 0.932 ± 0.13 , $N = 17$ sections, *Tcf4^{+/-tr}* 0.5235 ± 0.07 , $N = 16$ sections, $p = 0.0095$; **C2** WT 0.959 ± 0.232 , $N = 3$ animals, *Tcf4^{+/-tr}* 0.51 ± 0.09 , $N = 3$ animals, $p = 0.1464$). **D** Representative images showing PV+ INs in the BLA of WT and *Tcf4^{+/-tr}* mice. **D1** The density of PV+ INs was reduced in the BLA of *Tcf4^{+/-tr}* mice (**D1** WT 42.34 ± 4.74 , $N = 13$ sections, *Tcf4^{+/-tr}* 14.42 ± 2.37 , $N = 13$ sections, $p < 0.0001$; **D2** WT 42.68 ± 6.26 , $N = 3$ animals, *Tcf4^{+/-tr}* 14.85 ± 4.64 , $N = 3$ animals, $p = 0.0233$). **E** No effect of Tcf4 loss-of-function on the density of SST+ INs in the BLA of *Tcf4^{+/-tr}* mice (**E1** WT 193.3 ± 26.67 , $N = 12$ sections, *Tcf4^{+/-tr}* 180.3 ± 19.83 , $N = 12$ sections, $p = 0.6995$; **E2** WT 193.3 ± 33.3 , $N = 3$ animals, *Tcf4^{+/-tr}* 180.3 ± 27.24 , $N = 3$ animals, $p = 0.7776$). **F** The density of VIP+ INs was reduced in the BLA of *Tcf4^{+/-tr}* mice (**F1** WT 100.8 ± 6.32 , $N = 12$ sections, *Tcf4^{+/-tr}* 79.87 ± 4.41 , $N = 12$ sections, $p = 0.0126$; **F2** WT 100.8 ± 8.44 , $N = 3$ animals, *Tcf4^{+/-tr}* 79.87 ± 6.77 , $N = 3$ animals, $p = 0.1253$). **G** Representative images showing ChAT+ INs in the striatum of WT and *Tcf4^{+/-tr}* mice. **G1** The density of ChAT+ INs was reduced in the striatum of *Tcf4^{+/-tr}* mice (**G1** WT 41.19 ± 1.47 , $N = 24$ sections, *Tcf4^{+/-tr}* 31.18 ± 1.79 , $N = 24$ sections, $p < 0.0001$; **G2** WT 41.19 ± 2.38 , $N = 4$ animals, *Tcf4^{+/-tr}* 31.18 ± 2.55 , $N = 4$ animals, $p = 0.0285$). Stats mean \pm s.e.m., scale bars **A**, **G** = 400 μ m, scale bar **D** = 200 μ m.

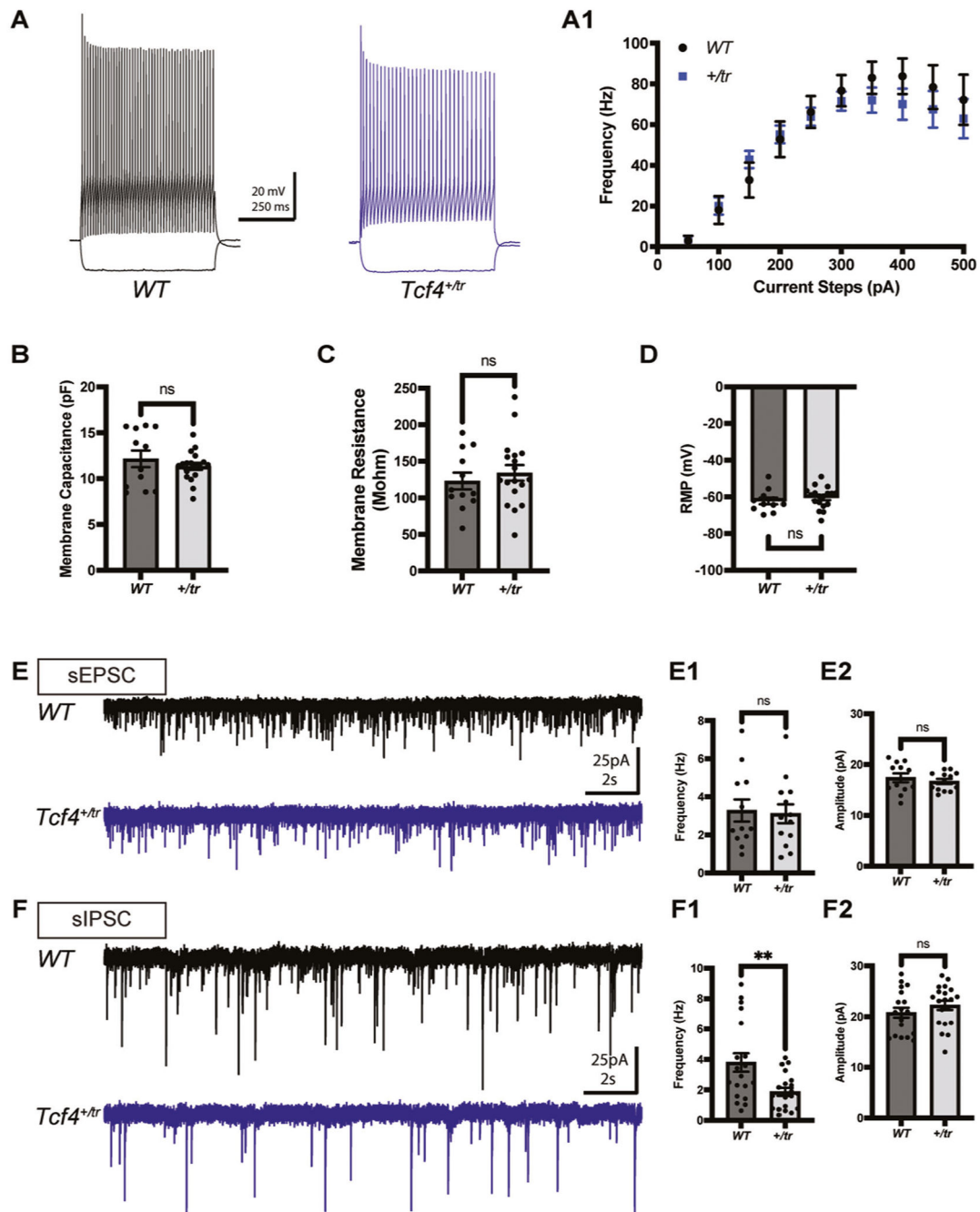


Fig. 5. Intrinsic and synaptic characteristics of PV + INs in the PTHS mouse model.

A Representative traces showing high frequency action potentials in response to current injections. **A1** No effect of TCF4 loss-of-function on action potential output in PV+ INs (ANOVA_{freq} $p = 0.3239$). **B** Membrane capacitance is not different by genotype (WT 12.17 ± 0.9 , $N = 12$ cells, HET 11.35 ± 0.38 , $N = 18$ cells, $p = 0.3538$). **C** Membrane resistance is not different by genotype (WT 123 ± 11.47 , $N = 12$ cells, HET 134.1 ± 10.76 , $N = 18$ cells, $p = 0.4994$). **D** Resting membrane potential is not different by genotype (WT -62.25 ± 1.81 , $N = 12$ cells, HET -60.41 ± 1.38 , $N = 18$ cells, $p = 0.4197$) **E** Representative traces showing

sEPSCs recorded from a PV + IN in a WT and *Tcf4^{+tr}* brain slice. **E1** The frequency of sEPSCs was not different by genotype (WT 3.28 ± 0.58 , $N = 12$ cells, HET 3.11 ± 0.5 , $N = 13$ cells, $p = 0.8259$). **E2** The amplitude of sEPSCs was not different by genotype (WT 17.4 ± 0.87 , $N = 12$ cells, HET 16.67 ± 0.51 , $N = 13$ cells, $p = 0.466$). **F** Representative traces showing sIPSCs recorded from PV+ INs in brain slices from WT and *Tcf4^{+tr}* mice. **F1** The frequency of sIPSCs was reduced in PV+ INs from *Tcf4^{+tr}* brain slices compared to WT PV+ INs (WT 3.79 ± 0.6 , $N = 19$ cells, HET 1.87 ± 0.26 , $N = 20$ cells, $p = 0.0051$). **F2** The amplitude of sIPSCs was not different by genotype (WT 20.79 ± 0.98 , $N = 19$ cells, HET 22.25 ± 0.9 , $N = 20$ cells, $p = 0.2819$).

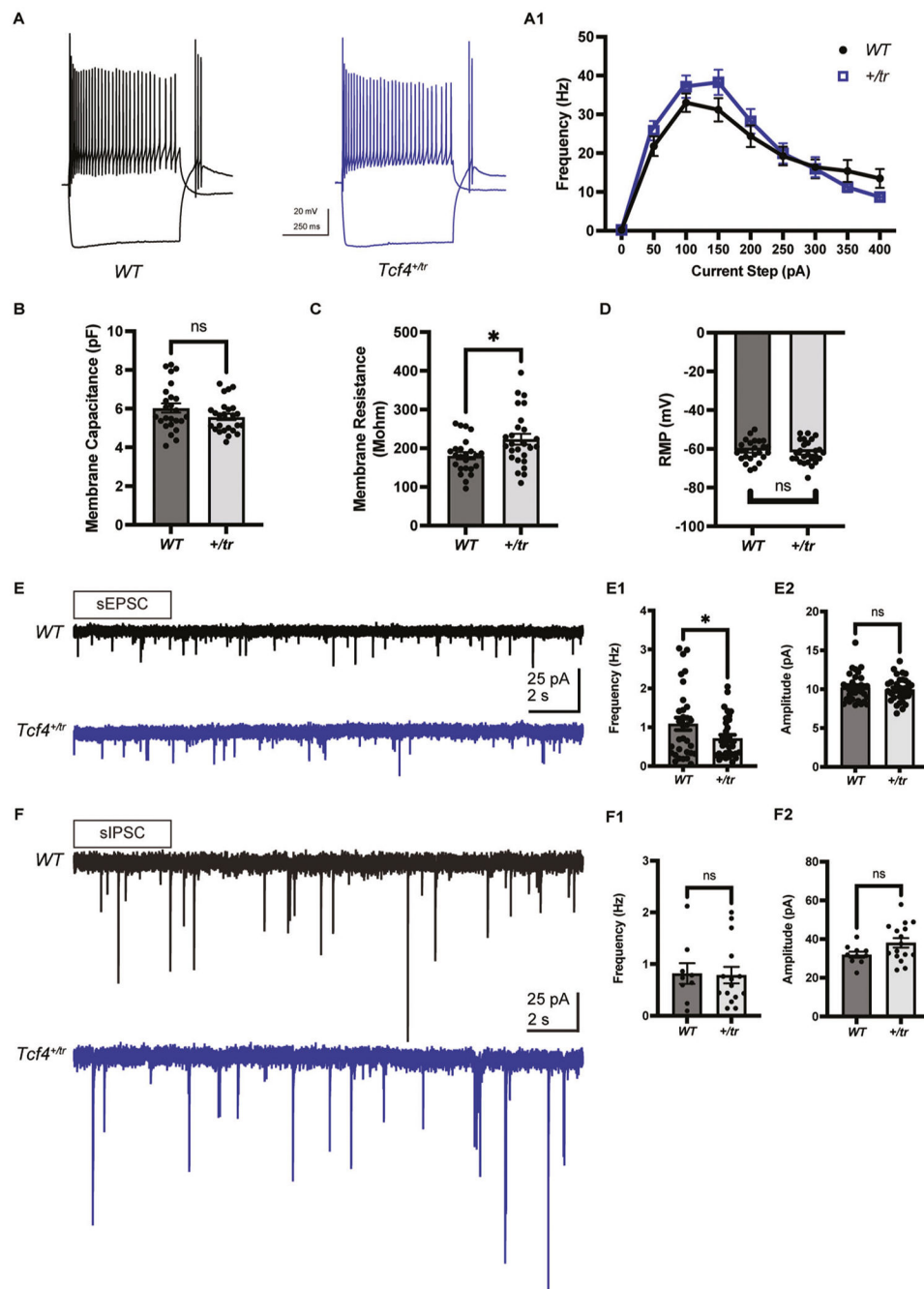


Fig. 6. Intrinsic and synaptic characteristics of VIP + INs in the medial prefrontal cortex of the PTHS mouse model.

A Representative traces showing action potentials in response to current injections. **A1** No effect of TCF4 loss-of-function on action potential output in VIP+ INs (ANOVA_{freq} $p = 0.3149$). **B** Membrane capacitance was not different by genotype (WT 6.05 ± 0.25 , $N = 24$ cells, $Tcf4^{+/-tr}$ 5.58 ± 0.17 , $N = 25$ cells, $p = 0.1125$). **C** Membrane resistance was increased in VIP+ INs from $Tcf4^{+/-tr}$ brain slices compared to WT VIP+ INs (WT 180 ± 9.24 , $N = 24$ cells, $Tcf4^{+/-tr}$ 227.1 ± 14 , $N = 25$ cells, $p = 0.0082$). **D** Resting membrane potential was

not different by genotype (WT -60.54 ± 1.04 , $N=24$ cells, $Tcf4^{+/tr}$ -61.67 ± 1.17 , $N=25$ cells, $p=0.4754$). **E** Representative traces showing sEPSCs recorded from a VIP + IN in a WT (black) and $Tcf4^{+/tr}$ (blue) brain slice. **E1** The frequency of sEPSCs was reduced in VIP+ INs from $Tcf4^{+/tr}$ brain slices compared to WT VIP+ INs (WT 1.09 ± 0.16 , $N=32$ cells, $Tcf4^{+/tr}$ 0.71 ± 0.09 , $N=34$ cells, $p=0.0415$). **E2** The amplitude of sEPSCs was not different by genotype (WT 10.21 ± 0.32 , $N=32$ cells, $Tcf4^{+/tr}$ 9.97 ± 0.26 , $N=34$ cells, $p=0.5593$). **F** Representative traces showing sIPSCs recorded from VIP+ INs in brain slices from WT (black) and $Tcf4^{+/tr}$ (blue) mice. **F1** The frequency of sIPSCs was not different by genotype (WT 0.82 ± 0.2 , $N=9$ cells, $Tcf4^{+/tr}$ 0.79 ± 0.16 , $N=15$ cells, $p=0.9079$). **F2** The amplitude of sIPSCs was not different by genotype (WT 32.31 ± 1.69 , $N=9$ cells, $Tcf4^{+/tr}$ 38.12 ± 2.6 , $N=15$ cells, $p=0.1228$).

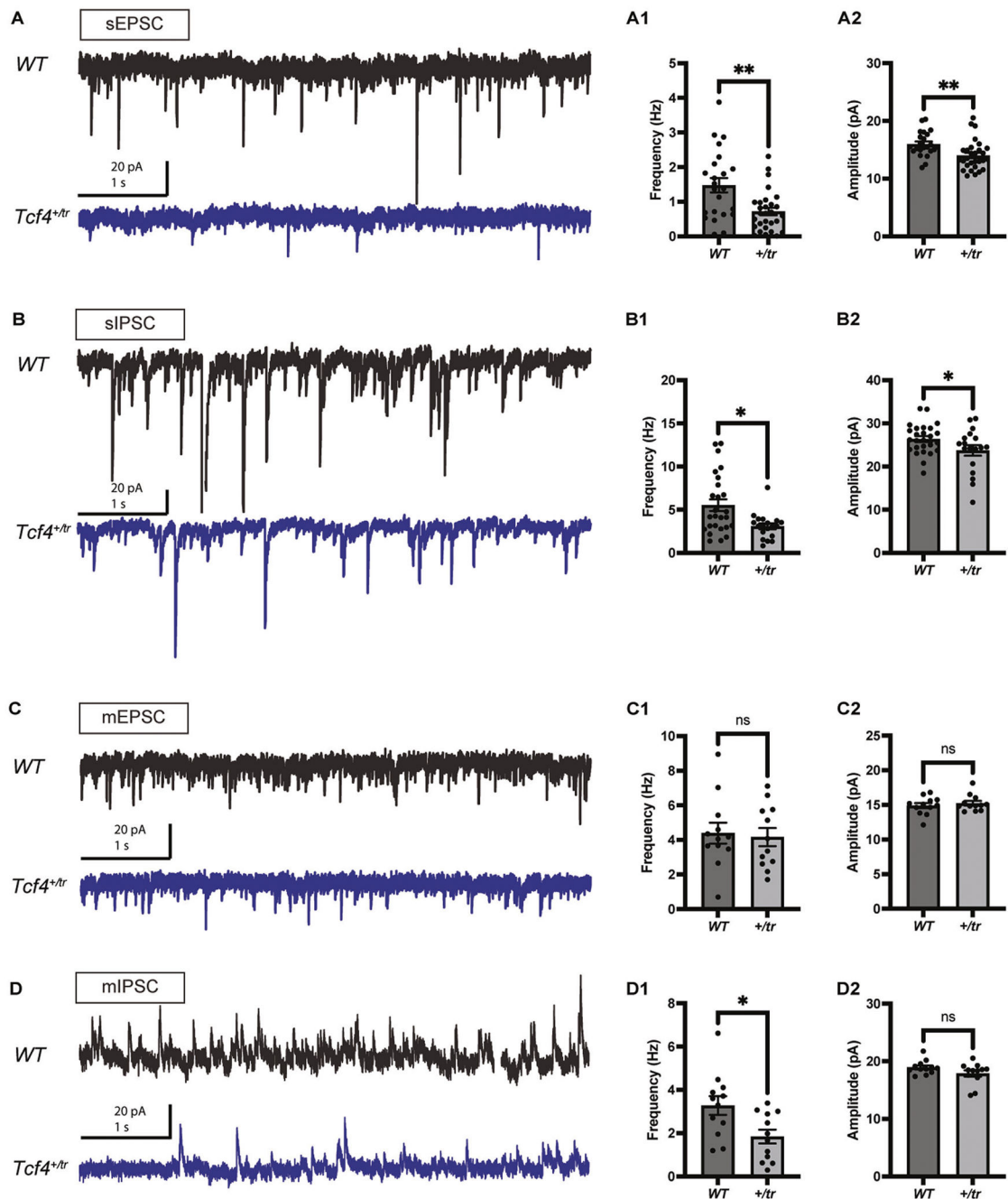


Fig. 7. Excitatory and inhibitory synaptic characteristics of medial prefrontal pyramidal neurons in the PTHS mouse model.

A Representative traces showing sEPSCs recorded from a pyramidal neuron in a WT (black) and *Tcf4*^{+/-tr} (blue) brain slice. **A1** The frequency of sEPSCs was reduced in pyramidal neurons from *Tcf4*^{+/-tr} brain slices compared to WT pyramidal neurons (WT 1.48 ± 0.21 , $N = 23$ cells, *Tcf4*^{+/-tr} 0.72 ± 0.11 , $N = 29$ cells, $p = 0.0012$). **A2** The amplitude of sEPSCs was reduced in pyramidal neurons from *Tcf4*^{+/-tr} brain slices compared to WT pyramidal neurons (15.99 ± 0.44 , $N = 23$ cells, *Tcf4*^{+/-tr} 14.02 ± 0.47 , $N = 29$ cells, $p = 0.0046$). **B**

Representative traces showing sIPSCs recorded from a pyramidal neuron in brain slices from WT (black) and *Tcf4^{+/-tr}* (blue) mice. **B1** The frequency of sIPSCs was reduced in pyramidal neurons from *Tcf4^{+/-tr}* brain slices compared to WT pyramidal neurons (WT 5.53 ± 0.68 , $N = 26$ cells, *Tcf4^{+/-tr}* 3.04 ± 0.36 , $N = 18$ cells, Mann–Whitney test $p = 0.0117$) **B2** The amplitude of sIPSCs was reduced in pyramidal neurons from *Tcf4^{+/-tr}* brain slices compared to WT pyramidal neurons (WT 26.37 ± 0.68 , $N = 26$ cells, *Tcf4^{+/-tr}* 23.74 ± 1.22 , $N = 18$ cells, $p = 0.0491$) **C** Representative traces showing mEPSCs recorded from a pyramidal neuron in a WT (black) and *Tcf4^{+/-tr}* (blue) brain slice. **C1** The frequency of mEPSCs was not different by genotype (WT 4.39 ± 0.6 , $N = 12$ cells, *Tcf4^{+/-tr}* 4.16 ± 0.53 , $N = 12$ cells, $p = 0.7765$). **C2** The amplitude of mEPSCs was not different by genotype (WT 14.9 ± 0.37 , $N = 12$ cells, *Tcf4^{+/-tr}* 14.97 ± 0.23 , $N = 11$ cells, $p = 0.8701$). **D** Representative traces showing mIPSCs recorded from a pyramidal neuron in brain slices from WT (black) and *Tcf4^{+/-tr}* (blue) mice. **D1** The frequency of mIPSCs was reduced in pyramidal neurons from *Tcf4^{+/-tr}* brain slices compared to WT pyramidal neurons (WT 3.28 ± 0.44 , $N = 12$ cells, *Tcf4^{+/-tr}* 1.84 ± 0.32 , $N = 12$ cells, $p = 0.0144$). **D2** The amplitude of mIPSCs was not different by genotype (WT 18.94 ± 0.34 , $N = 12$ cells, *Tcf4^{+/-tr}* 17.89 ± 0.55 , $N = 12$ cells, $p = 0.1173$).